Department of Precision and Microsystems Engineering

Design of a Nonlinear Stiffness Unit Cell Aided Magnetic Gravity Compensator

Timo Kouwenhoven

Report no : 2022.088
Coach : Marcin Kaczmarek
Professor : Hassan HosseinNia
Specialisation : Mechatronic System Design
Type of report : Master Thesis
Date : 5 December 2022

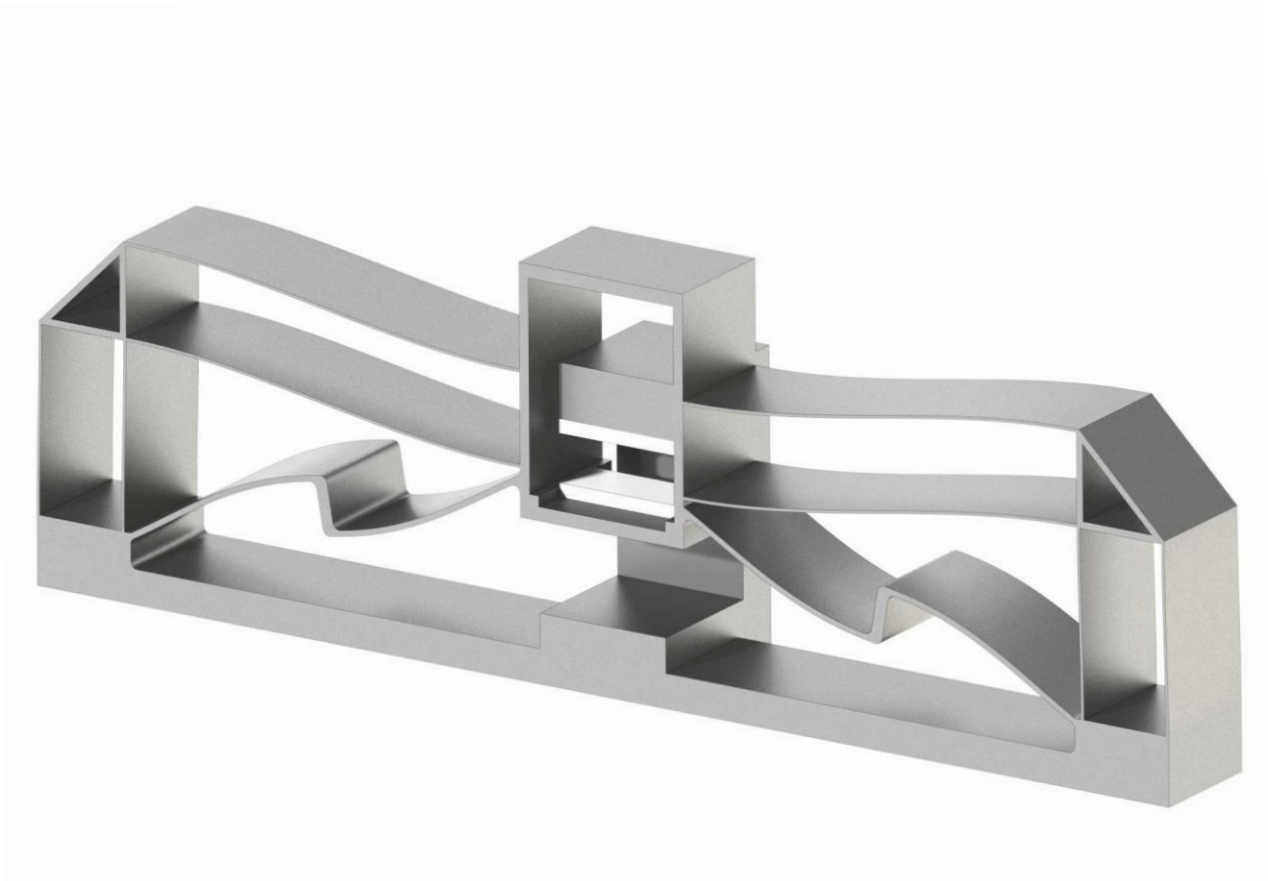

Design of a Nonlinear Stiffness Unit Cell Aided Magnetic Gravity Compensator

Author: Timo Kouwenhoven
Supervisor: Hassan HosseinNia
Daily Supervisor: Marcin Kaczmarek

December 5, 2022

Department of Precision and Microsystems Engineering

Preface

After a long road towards completing this project, I am happy to present my master thesis. What started as a vague concept of combining magnets and unit cells slowly turned into a tangible product. The process was definitely not easy, but I've learned a lot in a year's (and a bit) work. After many hours of COMSOL simulations, it was a big blow to find out my measurement results were completely different from the simulations. This inspired me to learn more about the working principle of the prototype to be able to predict what a change in parameters would do to the characteristics of system. As a result, the prototype was iteratively designed. This included making many 3d prints and doing a lot of lab measurements. It was difficult to stop making design iterations. There was always something to improve, but due to the limited amount of time, some concessions had to be made. I am, however, very happy with how the prototype turned out. Problems were solved with elegant solutions which makes for a very effective design.

First, I would like to thank Marcin Kaczmarek for his endless support as my daily supervisor. Without our meetings, I would have quickly drifted from my core goal, following impulsive ideas instead. This would have resulted in me never finishing this project. Second, I would like to thank Hassan HosseinNia for his out-of-the-box thinking throughout the project and for the kind support during tough times. Finally, I would like to thank Chao Song for his feedback on the writing of my paper.

Abstract

A novel nonlinear stiffness unit cell aided magnetic gravity compensator is proposed for the purpose of isolating low-frequency vibrations. A negative stiffness magnet setup is combined with a compliant unit cell with tailored nonlinear force-displacement characteristics. This combination offers a large range of motion featuring low stiffness, a high force density, and passive stability, creating a large vertical displacement passive magnetic gravity compensator (LVDPMGC). The passive stability of the system eliminates the need for active stabilization, reducing costs and complexity. An adjustable load-bearing capacity can be obtained by changing the number of unit cells, increasing scalability compared to conventional magnetic gravity compensators (MGC's) which have a fixed load-bearing capacity. The stiffness characteristics of the unit cell and magnet setup are analysed with FEM, showing which parameters influence system performance. Parameters are iteratively adjusted after which a prototype is manufactured and tested. The experimental results show that the unit cell can effectively stabilize the magnet setup while increasing the low stiffness range of motion, force density, and scalability compared to conventional MGC's.

Contents

1 Introduction

Passive vibration isolation is a cost-effective way to attenuate unwanted vibrations. The isolation performance of a linear passive system is highly dependent on its stiffness, which directly affects the resonance frequency of the system. A low resonance frequency is critical for isolating a wide range of frequencies. Due to gravitational sagging [1], there is a limit to the minimum stiffness of a linear isolator. This makes these systems a poor choice for low-frequency vibration isolation.

Currently, there is a growing interest in quasi-zero stiffness (QZS) systems due to their excellent performance at a wide range of frequencies. A high static stiffness minimizes gravitational sagging, while a low dynamic stiffness ensures vibration attenuation at low frequencies. This low dynamic stiffness is obtained by counteracting positive stiffness with negative stiffness, which creates a zero-stiffness region present around the operating point.

There are many mechanisms which feature QZS characteristics. Early designs achieved QZS by providing negative stiffness to a positive stiffness spring bearing the isolation mass [2]. Further developments focused on increasing the force density of the design [3], increasing the range of motion around the operating point [4, 5], and miniaturizing the design into simple compliant unit cells [6, 7, 8].

Certain magnet setups also feature QZS characteristics. These setups are known as magnetic gravity compensators (MGC) and feature positive and negative stiffness regions. A zero-stiffness point is located between these regions. Some properties inherent to MGC technology make them interesting for high-precision applications. A high force density allows for a compact design and large load applications. The technology can achieve very high performance, effectively isolating nearly all frequencies. Finally, Contactless operation eliminates friction, improving repeatability and ensuring no particle contamination [9].

1.1 Motivation

MGC's have been studied extensively in the past decades [10, 11, 12, 13]. Several limitations prevent wide-scale implementation, however:

- The magnets require active control to stay at the operating point. This is expensive to implement, and the heat generated by the active control can affect the performance of high-precision devices.
- The QZS characteristics cause the system to only achieve high performance for a small range of motion, deteriorating performance at higher vibration amplitudes.
- The isolation mass of an MGC can not be changed easily since the device can only achieve high performance around the operating point which has a fixed load-bearing capacity. A change in isolation mass often requires a complete redesign of the magnets and active control.

Current research focuses on solving the above-mentioned limitations. Berkhof et al. [14] created a passively stable MGC by stabilizing a magnet setup with positive stiffness linear flexures. Mofidian et al. [15] and Dong et al. [16] used negative stiffness magnet setups to lower the total stiffness of a spiral spring. Zhang et al. [17, 18] minimized nonlinearity in the system by combining multiple magnet setups with opposite stiffness. Finally, Argiro et al. [19] designed a long-stroke MGC while maintaining low stiffness.

No single design has yet been proposed that effectively combines the stabilization of MGC technology with an increased range of motion, a high force density, and increased scalability.

1.2 Research Objective

In this research, a magnet setup is combined with a nonlinear stiffness unit cell composed of a novel stepped flexure design and a guiding stage, which together oppose the stiffness of a magnet setup. The new design should be passively stable, exhibit low stiffness for a large range of motion, and be easily scalable, creating a large vertical displacement passive magnetic gravity compensator (LVDPMGC). The research question can be formulated as follows:

"How can a nonlinear stiffness unit cell stabilize a magnet setup while increasing its range of motion and scalability?"

To achieve this, some sub-objectives have been formulated:

1. Find a magnet setup with favourable stiffness characteristics when combined with a unit cell.
2. Develop a unit cell design composed of nonlinear stiffness stepped flexures and a guiding stage to oppose the stiffness of the magnet setup.
3. Validate the LVDPMGC through experiments.

1.3 Outline

This research is structured as follows: Chapter 2 includes a paper which shows the scientific significance of the new LVDPMGC. Then, in chapter 3, measurements of both the magnets and unit cell are discussed. Chapter 4 shows the working principle of an earlier version of the LVDPMGC and compares it to the new design. Chapter 5 discusses the fabrication details of the prototype. Chapter 6 shows the performance of the LVDPMGC. Chapter 7 discusses the results and limitations of the evaluation methods from chapter 6 in more detail. Finally, chapter 8 concludes this research and gives recommendations for future research.

2 Design of a Nonlinear Stiffness Unit Cell Aided Magnetic Gravity Compensator

Design of a Nonlinear Stiffness Unit Cell Aided Magnetic Gravity Compensator

T. Kouwenhoven[1] M.B. Kaczmarek[2] C. Song[3] S.H. HosseinNia[4]

[1]timo.kouwenhoven@hotmail.com [2]M.B.Kaczmarek@tudelft.nl
[3]C.Song@tudelft.nl [4]S.H.HosseinNiaKani@tudelft.nl

Delft University of Technology

Abstract

A novel nonlinear stiffness unit cell aided magnetic gravity compensator is proposed for the purpose of isolating low-frequency vibrations. A negative stiffness magnet setup is combined with a compliant unit cell with tailored nonlinear force-displacement characteristics. This combination offers a large range of motion featuring low stiffness, a high force density, and passive stability, creating a large vertical displacement passive magnetic gravity compensator (LVDPMGC). The passive stability of the system eliminates the need for active stabilization, reducing costs and complexity. An adjustable load-bearing capacity can be obtained by changing the number of unit cells, increasing scalability compared to conventional magnetic gravity compensators (MGC's) which have a fixed load-bearing capacity. The stiffness characteristics of the unit cell and magnet setup are analysed with FEM, showing which parameters influence system performance. Parameters are iteratively adjusted after which a prototype is manufactured and tested. The experimental results show that the unit cell can effectively stabilize the magnet setup while increasing the low stiffness range of motion, force density, and scalability compared to conventional MGC's.

1 Introduction

Passive vibration isolation is a cost-effective way to attenuate unwanted vibrations. As linear isolators lack the ability to attenuate low-frequency vibrations, there is a growing interest in quasi-zero stiffness (QZS) systems to isolate sensitive equipment. These systems can attenuate a wide range of frequencies due to their high static and low dynamic stiffness. This low dynamic stiffness is obtained by counteracting positive stiffness with negative stiffness, which creates a zero-stiffness region present in a small range of motion around the operating point.

There are many mechanisms which feature QZS characteristics. Early designs achieved QZS by combining negative stiffness elastic elements with a positive stiffness spring bearing the isolation mass [1]. Further developments in the field were focussed on three factors. The first goal was to increase the magnitude of the negative stiffness for small displacements [2], introducing the possibility of incorporating larger positive stiffness springs, effectively increasing the force density. Secondly, a more constant stiffness for an increased range of motion was obtained [3, 4]. Finally, the designs were miniaturized by changing the complex mechanisms to simple compliant unit cells [5, 6, 7].

Certain magnet setups also feature QZS characteristics. These setups are known as magnetic gravity compensators (MGC's) and feature positive and negative stiffness regions. A zero-stiffness point is located between these regions. Some properties inherent to MGC technology make them interesting for high-precision applications. A high force density allows for a compact design and large load applications. The technology can achieve very high performance, isolating nearly all frequencies. Finally, contactless operation eliminates friction, improving repeatability and ensuring no particle contamination [8].

Hol et al. [9] has written an extensive review on the design and optimization of MGC's. Janssen et al. [10] and Zhang et al. [11] optimized MGC designs for large-load applications. Zhu et al. [12] focused on the stability of an MGC for the design of an active stabilisation system. Zhang et al. [13] created a cylindrical MGC with a new semi-analytical method to accurately model magnets.

Some limitations prevent the wide-scale implementation of MGC's. Firstly, the magnets require active control to stay at the operating point. This increases the cost of a system, and the heat generated by the active control can affect the performance of high-precision devices. Secondly, the QZS characteristics cause the system to only achieve high performance for a small range of motion, deteriorating performance at higher vibration amplitudes. Lastly, MGC's can only achieve high performance around the operating point which has a fixed load-bearing capacity. The scalability of the current systems is limited because a change in load often requires a complete redesign of the magnets and active control.

Some recent studies have been conducted to eliminate the drawbacks of MGC's. Argiro et al. [14] designed a long-stroke MGC while maintaining low stiffness. Zhang et al. [15] used two magnet configurations with opposite stiffness to create a near zero-stiffness isolator. Zhang et al. [16] incorporated two magnet configurations with opposing stiffness in a compact design, increasing the effective load-bearing capacity while maintaining a large stroke.

Another way to eliminate the drawbacks of MGC technology is by combining a magnet setup with mechanical structures. Xu et al. [17] changed the mechanical springs in the design of Platus et al. [1] by a magnet setup exhibiting negative stiffness. Mofidian et al.[18] and Dong et al. [19] used negative stiffness magnet setups to lower the total stiffness of a spiral spring. Finally, Berkhof et al. [20] created a passively stable MGC by stabilizing a magnet setup with positive stiffness linear flexures.

To date, no single design effectively combines the passive stabilization of MGC technology, an increased range of motion featuring low stiffness, a high force density, and increased scalability. In this paper a new design is proposed, combining a negative stiffness magnetic spring with a variable stiffness unit cell. The design solves all of the above-mentioned issues, creating a large vertical displacement passive magnetic gravity compensator (LVDPMGC). The performance of the LVDPMGC is validated by static and dynamic test data.

This paper is organized as follows: In section 2, the configuration of the proposed LVDPMGC is discussed. In section 3, the working principle of the LVDPMGC is described. This includes explaining the different modelling techniques used to simulate individual parts of the LVDPMGC. In section 4, a parameter analysis shows the influence of different parameters on the system behaviour. In section 5, a prototype of the LVDPMGC is validated with static and dynamic experiments. In section 6, the results are discussed in more detail. Finally, the paper is concluded in section 7.

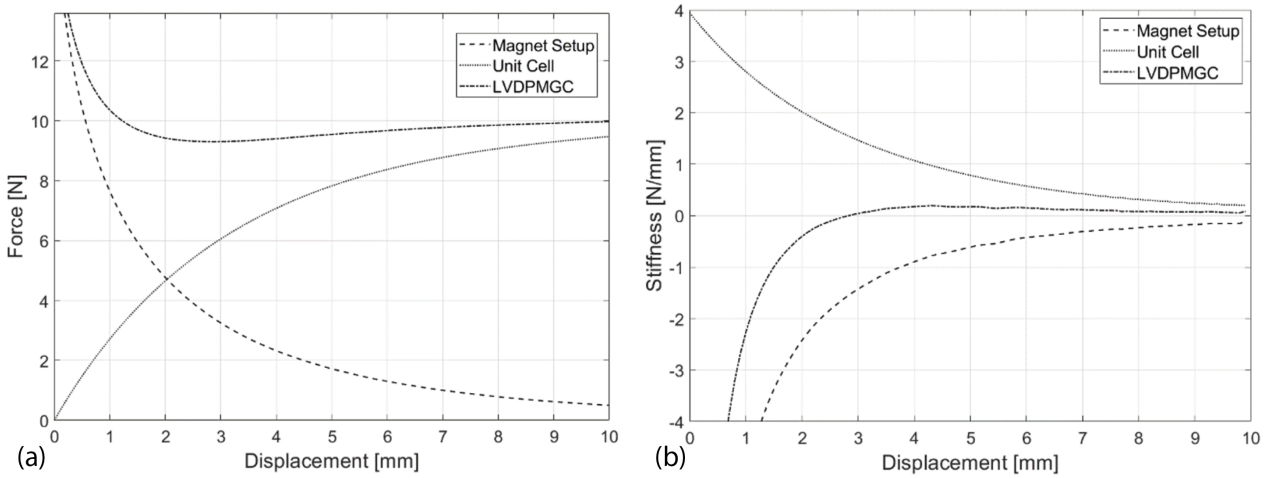

Figure 1: (a) Force characteristics of the magnet setup, unit cell, and LVDPMGC, (b) Stiffness characteristics of the magnet setup, unit cell, and LVDPMGC

2 Configuration of the LVDPMGC

The configuration of the LVDPMGC is shown in figure 2. It is composed of a variable stiffness unit cell housing a magnet setup consisting of a stator magnet and a mover magnet. The stator magnet is rigidly connected to the base of the unit cell while the mover magnet is connected to a set of stepped flexures and a guiding stage.

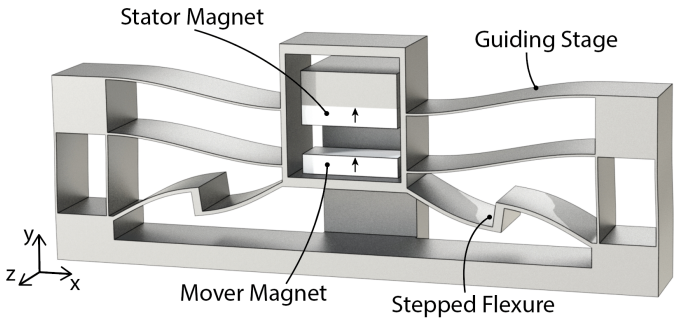

Figure 2: Configuration of the LVDPMGC

The mover magnet is attracted by the top magnet which creates a nonlinear upwards force with increasing negative stiffness for decreasing gap size. The stepped flexures and the guiding stage work together to achieve near equal and opposite stiffness to the magnet setup while exerting a force in the same direction as the magnet setup. Figure 1 shows the force and stiffness plots of the magnet topology, variable stiffness unit cell, and their combination.

To restrict any unwanted degrees of freedom, a linear guiding stage is connected to both sides of the mover magnet. A guiding stage consists of two sets of parallel flexures, restricting all rotations and movement in z-direction. The stepped flexures constrain the system in x-direction, leaving one degree of freedom in y-direction. This allows vertical travel of the mover magnet. To stabilize the system in y-direction, the first 3mm of motion are blocked by mounting a spacer between the magnets. This leaves a system with a 7mm low-stiffness range of motion.

The LVDPMGC is compared to a conventional MGC setup used in [11, 12, 15]. It consists of a floating magnet positioned between two stationary magnets. The configuration uses equal magnet dimensions to the magnets used in the LVDPMGC. Its force and stiffness plots, simulated with the charge model, discussed in section 3.1, are shown in figure 3. Over the working range, the LVDPMGC manages to increase the load-bearing capacity and the low stiffness range of motion compared to the conventional MGC setup. Furthermore, the LVDPMGC features a stable range of motion, while the working range of the conventional MGC includes a large unstable region. This passive way of stabilization eliminates the need for active control and increases the scalability of the system by enabling multiple unit cells to work together to create an adjustable load-bearing capacity without the need for a redesign of the entire system.

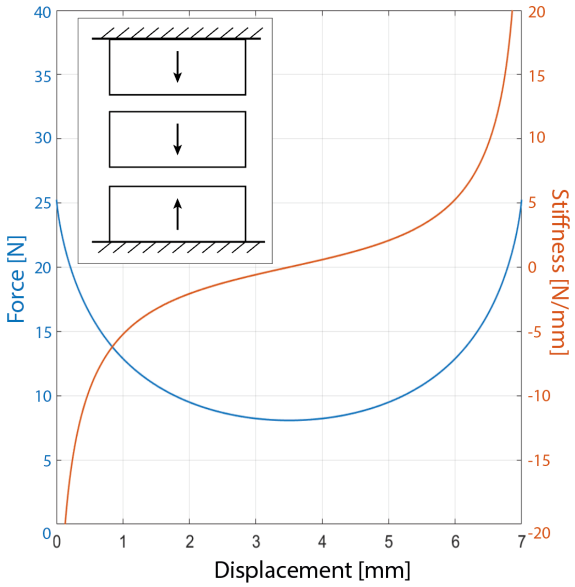

Figure 3: Force and stiffness characteristics of a conventional MGC setup

3 Working Principle of the LVDPMGC

In this section, the working principle of the individual components in the LVDPMGC are discussed. The charge model is introduced for the modelling of magnets. Then, a mechanical analysis of the unit cell shows the behaviour of both the guiding stage and the stepped flexures.

3.1 Modelling of the Negative Stiffness Magnet Setup

The force between magnets can be analytically calculated with the surface charge model [21], where a permanent magnet can be represented by positive and negative charges on its poles. The general equation for modelling the force between two cuboid magnets, depicted in figure 4, is given by equation 1.

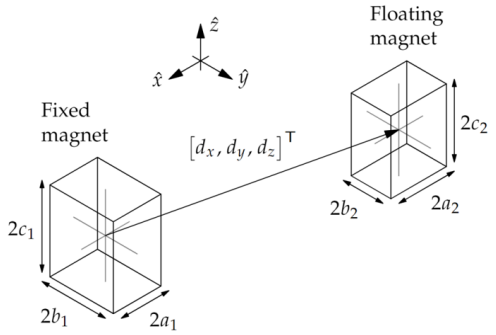

Figure 4: Magnet geometries used in the charge model

$$\boldsymbol{F}_{z,z} = \frac{B_{r1}B_{r2}}{4\pi\mu_0} \sum_{i,j,k,l,p,q \in \{0,1\}^6} \boldsymbol{\phi}_{z,z}(\boldsymbol{\delta}_{i,j,k,l,p,q}) \cdot [-1]^{i+j+k+l+p+q} \tag{1}$$

where

$$\boldsymbol{\delta}_{i,j,k,l,p,q} = \begin{bmatrix} \delta_{x(i,j)} \\ \delta_{y(k,l)} \\ \delta_{z(p,q)} \end{bmatrix} = \begin{bmatrix} d_x - a_1[-1]^i + a_2[-1]^j \\ d_y - b_1[-1]^k + b_2[-1]^l \\ d_z - c_1[-1]^p + c_2[-1]^q \end{bmatrix} \tag{2}$$

describes the distance between the corners of the two magnets. $Br1$ and $Br2$ denote the remanence of the two magnets and μ_0 is the permeability of free space. ϕ_{zz} is a function of δ and is given in [21].

The main assumption is that all materials inside the model have a relative permeability of one. In this case, the absolute force between magnets with parallel magnetization and anti-parallel magnetization is identical. Magnets, which have a relative permeability greater than one, will be stronger in attraction than repulsion. This is due to the field inside the magnet increasing if the external field aligns with the magnetization direction and decreasing if the external field opposes the magnetization direction. For small separations, the working point of a magnet can change, affecting the force between magnets. This effect is especially visible in complex magnet setups where magnets with different magnetizations operate close to each other, as can be seen in [16].

Due to the simple magnet setup used in this research, and the relative permeability of the magnets in question being very close to one, there is only a small difference between the results of the charge and FEM model, shown in figure 5. In this case, the charge model is sufficient to calculate the force of the negative stiffness magnetic spring.

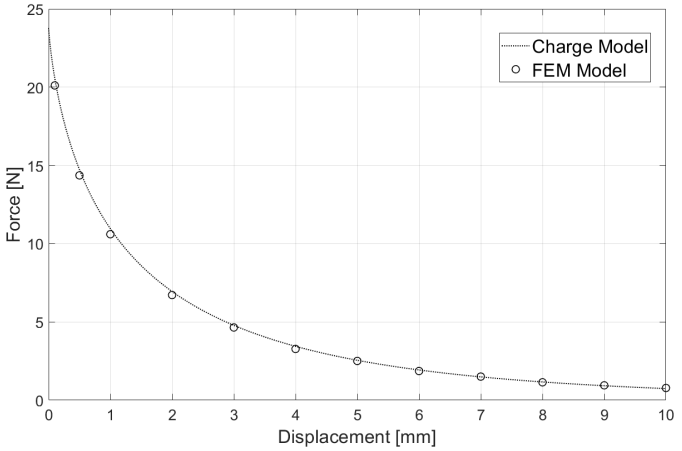

Figure 5: Force characteristics of two magnets in attraction

3.2 Mechanical Analysis of the Unit Cell

The characteristics of the unit cell are influenced by both the stepped flexures and the guiding stage. Where the stepped flexures determine the main force-displacement characteristics of the LVDPMGC, the guiding stage offers positive stiffness in y-direction, stabilizing the system and increasing the low stiffness range of motion.

Figure 6 shows the schematic of a guiding stage and a stepped flexure. Both are constrained in x-direction due to the symmetry in the unit cell and the high stiffness of the stepped flexures in this direction.

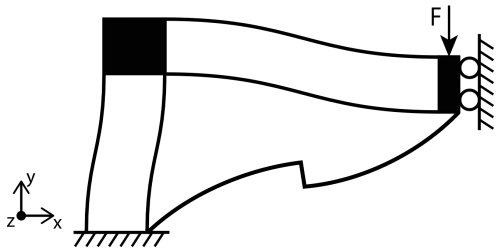

Figure 6: Schematic of a single guiding stage and a stepped flexure

A stepped flexure consists of two equally sized parallel sub-flexures connected at their endpoints. A guiding stage is rigidly connected to the free ends of the stepped flexure. It consists of two sets of parallel flexures, guiding the stepped flexure.

3.2.1 Stepped Flexures

A stepped flexure features an inflection point I, which lies halfway through the stepped flexure. The inflection point, shown in figure 7a, has zero curvature due to symmetry. The Euler-Bernoulli theory states that the bending moment in a beam depends on the curvature of the beam:

$$M = -EI\frac{d^2w}{dx^2} \tag{3}$$

With M the moment, EI the flexural rigidity, and $\frac{d^2w}{dx^2}$ the curvature of the beam.

As the curvature at the inflection point is zero, we can conclude that the moment at this point is also zero. We can therefore consider a single sub-flexure with a load F and a reaction force R acting on a beam attached to the end of the sub-flexure, shown in figure 7b. The reaction force is a result of the constraint in x-direction. Together with load F, they create a moment around the endpoint of the sub-flexure. This moment helps with initial buckling and smoothens the force of the unit cell.

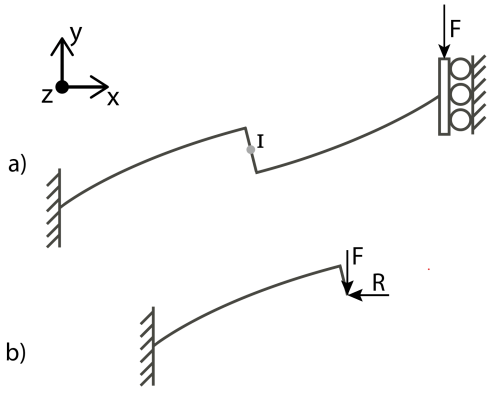

Figure 7: Schematic of a stepped flexure

As the stepped flexure moves down, the working angle will grow smaller, decreasing the vertical component of the flexure force. This effect, together with the sub-flexures gradually losing stiffness as they bend, will cause negative stiffness in the system for larger displacements. Very large step sizes only show positive stiffness for the entire range of motion. This is due to the moment R growing larger for a certain force F, loading the flexures in bending and decreasing the buckling effects. To accurately model the negative stiffness of the stepped flexures, a 3d FEM method is used.

3.2.2 Guiding Stage

The guiding stage consists of two sets of parallel flexures. A single flexure can constrain three degrees of freedom, leaving flexibility in two rotational degrees of freedom and a single translational degree of freedom. By adding a second flexure in parallel, two extra rotational degrees of freedom are constrained, leaving the system with a single translational degree of freedom along the thin side of the flexures. The second set of parallel flexures, mounted perpendicular to the first set, creates a system with two degrees of freedom.

The vertical displacement of the guiding stage depends on both sets of flexures. When looking at a single horizontal flexure, depicted in figure 8b, bending is influenced by external force Fy, the reaction force Fx, and a resulting moment M1. The reaction force is a result of the shortening of the horizontal flexure under loading, causing a displacement Δx. This displacement bends the vertical flexure, shown in figure 8a, creating the reaction force. When all forces are known, the displacement of the guiding stage can be calculated by adding the vertical displacement of both the horizontal and vertical flexures, Δy1 and Δy2. Due to the large displacements of the flexures and the complexity of the coupled system, a 3d FEM method is used to calculate the force characteristics of the guiding stage.

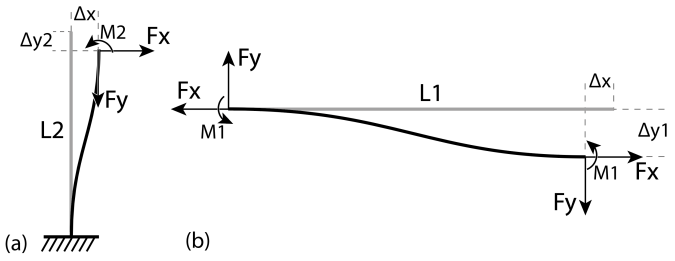

Figure 8: a) Free body diagram of a vertical flexure, b) free body diagram of a horizontal flexure

4 Parameter Analysis

The LVDPMGC has many individual parameters which all play a role in the isolation performance of the system. In this section, the effect of each parameter is analysed and the final parameters of the prototype are obtained.

4.1 Magnet Setup

The magnet setup can be simulated using the charge model introduced in section 3.1. The aspect ratio of each magnet, the measure of the magnet height compared to its length and width, influences the force characteristics of the magnet setup. Figure 9 shows the force and stiffness characteristics of the magnet setup for a varying aspect ratio.

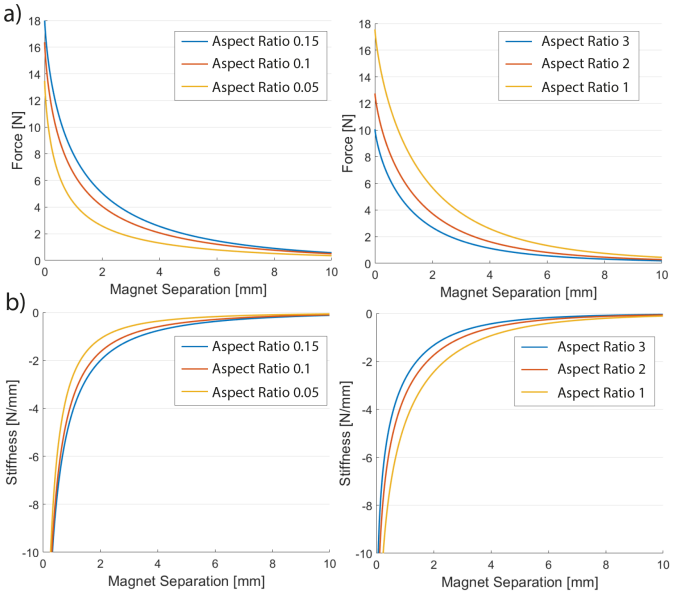

Figure 9: a) Force characteristics of a magnet setup with variable aspect ratio, b) Stiffness characteristics of a magnet setup with variable aspect ratio

A magnet with a very small aspect ratio has a very steep decline in force for small separations while larger aspect ratios will have a more gradual decline in force. The unit cell has a more gradual decrease in stiffness, making small aspect ratio's not suitable for the LVDPMGC. A magnet with a very large aspect ratio decreases the maximum force between the magnets, decreasing force density. An optimal aspect ratio can therefore be found in which the magnet setup has a gradual decrease in stiffness and the force density of the magnet setup is high.

Another important parameter for the magnet setup is the initial magnet separation, indicating the separation between the magnets when the unit cell is in its neutral position. Increasing initial magnet separation can help decrease the magnitude of the negative stiffness for small displacements. This can be beneficial because the initial negative stiffness of the magnet setup is much larger than the initial positive stiffness of the unit cell, resulting in a negative stiffness region at small displacements for the LVDPMGC.

4.2 Unit Cell

The stepped flexures and guiding stage are separately analysed to show the effect of their parameters. The unit cell depth in z-direction is constant over both the stepped flexures and the guiding stage. It linearly affects the total stiffness of the system. The depth of the unit cell is very important for the out-of-plane stability of the LVDPMGC and should therefore not be too small.

4.2.1 Stepped Flexures

Figure 11 shows the parameters of interest for a stepped flexure, with θ the angle of the stepped flexure, L the length of a sub flexure, S the step size, and t the thickness of a sub flexure. Figure 10 shows the influence of changing these parameters on the force and stiffness characteristics of the unit cell while other parameters stay constant.

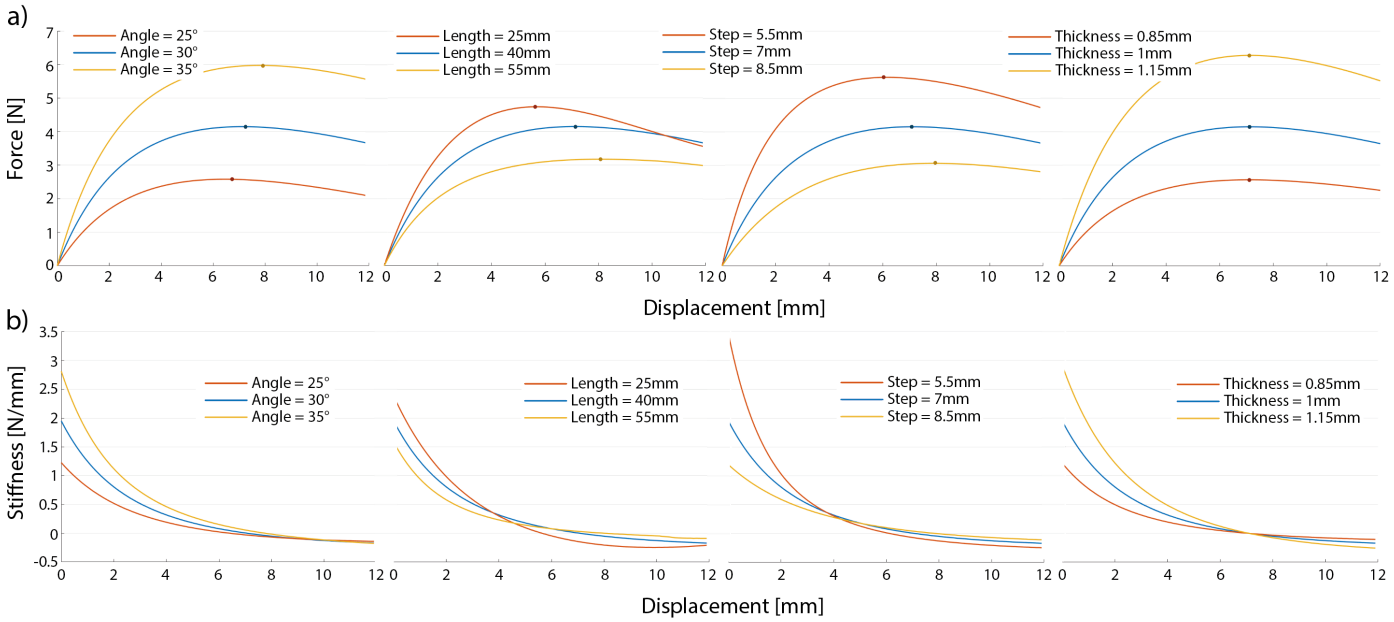

Figure 10: a) Force characteristics of the stepped flexures for varying parameters, b) Stiffness characteristics of the stepped flexures for varying parameters

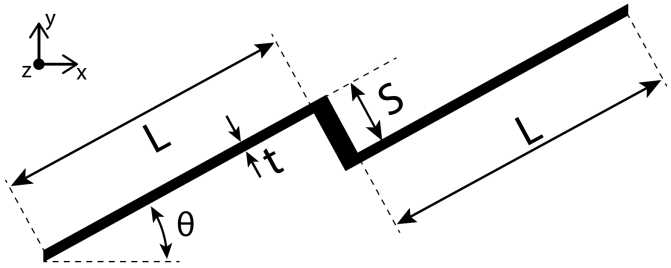

Figure 11: Parameters of a stepped flexure

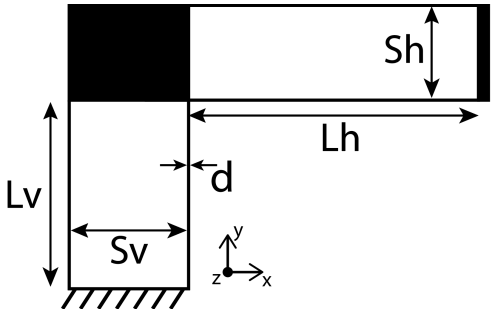

Figure 12: Parameters of a guiding stage

The angle of the stepped flexure greatly influences the initial stiffness of the unit cell while having minimal effect on the stiffness at large displacement. The zero-stiffness point, depicted by a dot in the force plots, shifts for increasing angles. The zero-stiffness point is a good indication of the working range of the LVDPMGC due to its large influence on the range at which the negative stiffness of the nonlinear magnetic spring can be neutralized.

Increasing the sub-flexure length shifts the zero-stiffness point to the right, just as increasing the angle. Opposite to the angle, however, increasing the length decreases the initial stiffness. Stiffness at large displacement can also be changed by the sub-flexure length.

The step size has a much greater influence on the initial stiffness of the unit cell compared to the effect on the zero-stiffness point and large displacement stiffness. It can be used to match the initial stiffness of the nonlinear magnetic spring to obtain near-zero stiffness at small displacements.

Finally, the sub-flexure thickness changes the overall force and stiffness of the unit cell. It does not influence the location of the zero-stiffness point.

4.2.2 Guiding Stage

Figure 12 shows the parameters of interest for the guiding stage.

The parameters of the guiding stage should meet the following requirements:

$$\begin{aligned} Lh_{min} \leq Lh \leq Lh_{max} \\ Lv_{min} \leq Lv \leq Lv_{max} \end{aligned} \tag{4}$$

with Lh_{min} and Lv_{min} the x- and y-dimensions of the stepped flexures. Lh_{max} and Lv_{max} should be chosen to maintain reasonable unit cell dimensions.

The force and stiffness characteristics for varying flexure lengths are shown in figure 13. Each figure shows a variable flexure length while the other parameters stay constant. It can be seen that the length of the horizontal set of flexures affects the overall stiffness of the guiding stage while the length of the vertical set of flexures affects the stiffness at large displacement

Besides the flexure length, the force characteristics of the guiding stage can also be changed by adjusting the flexure thickness d. Changing the thickness affects the overall stiffness of the guiding stage.

To maintain high stiffness in rotation and z-translation, important for the stabilization of the unit cell, certain parameters are of importance. The thickness and length of each flexure determine the buckling load of the flexure. To avoid buckling, flexures should not be too thin or too long. The flexure separations Sh and Sv affect the rotational stiffness of each set of flexures. For the vertical set of flexures, this affects the rotational stiffness around y and z, while for the horizontal set of flexures, this affects the rotational stiffness around x and z. To maintain a balanced system, these design requirements must be taken into account.

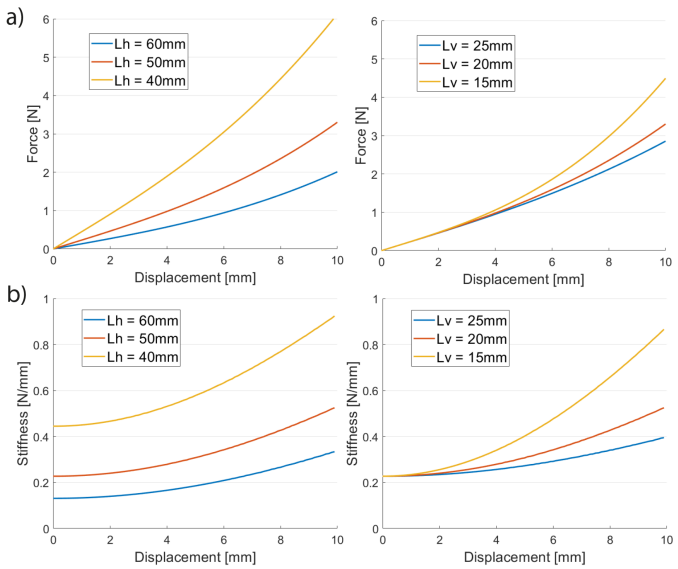

Figure 13: a) Force characteristics of the guiding stage for varying flexure length, b) Stiffness characteristics of the guiding stage for varying flexure length

4.3 Final Design Parameters

A set of design objectives is obtained from the results of the unit cell and magnet simulations, shown in equation 5.

$$\begin{aligned} 0 < Ky < K_{limit} \\ Dy > D_{min} \end{aligned} \tag{5}$$

With Ky the stiffness of the LVDPMGC in y-direction and Dy the vertical displacement for which this stiffness can be achieved. Simulations showed that a low stiffness of 0.2 N/mm was possible for a large vertical displacement of 5mm, setting the values for K_{limit} and D_{min}.

No optimization function was used due to the difficulty of accurately modelling the unit cell. Parameters were manually adjusted until the requirements were met. The final parameters are shown in table 1.

Magnets	
Length	20mm
Width	8mm
Height	2mm
Initial Separation	0.1mm

Unit Cell	
Material	PLA
Depth	18mm

Stepped Flexures	
θ	29.33 deg
L	34.06mm
S	7.7mm
t	0.85mm

Guiding Stage	
Lh	63mm
Lv	26mm
Sh	11mm
Sv	13mm
d	0.63mm

Table 1: Final parameters for the LVDPMGC

5 Experiments

With the knowledge from section 4 a unit cell was fabricated with Fused Deposition Modelling. A setup, shown in figure 14, consisting of a positioning stage equipped with a force sensor was used to measure the force-displacement characteristics of the unit cell, magnet setup, and LVDPMGC.

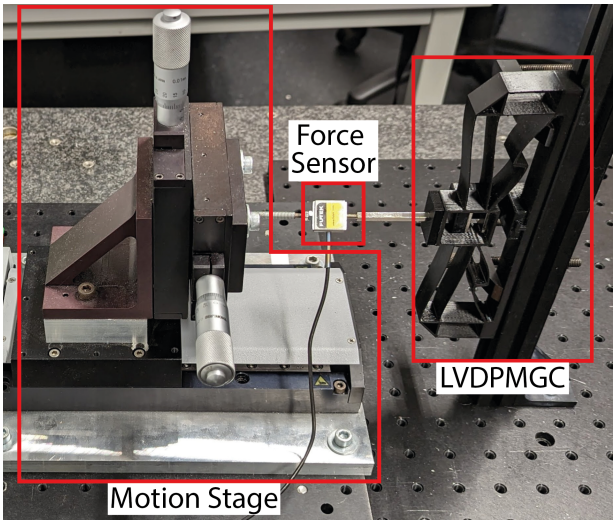

Figure 14: Motion stage equipped with a force sensor measuring the force-displacement characteristics of the LVDPMGC

Figure 15 shows the levitation force and stiffness of the horizontal measurement in which gravity does not influence the force characteristics. The measurement result of the LVDPMGC agrees well with the sum of the unit cell and magnet setup measurements. The residual error can be explained by assembly inaccuracies. The LVDPMGC measures a variation in force of only 0.5 N for a large range of 7mm with a passive levitation force of 9.6 N. The maximum stiffness in this range is below 0.12 N/mm.

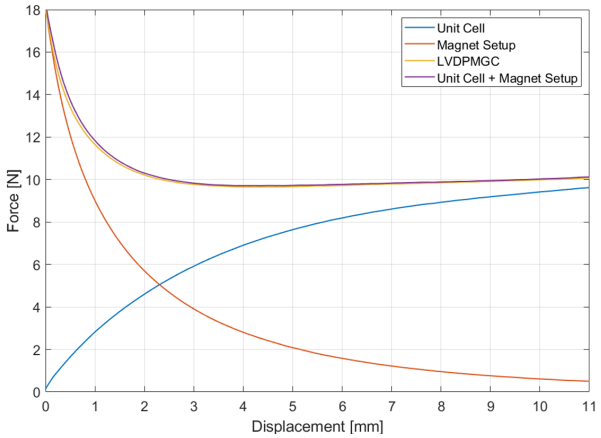

Figure 15: Force characteristics of the unit cell, magnet setup, their combination, and the LVDPMGC

To determine the eigenfrequency and damping of the LVDPMGC, the unit cell is pulled to its lowest position and then released. The position of the unit cell is measured with a camera which is calibrated with a measurement tape. The setup is shown in figure 16.

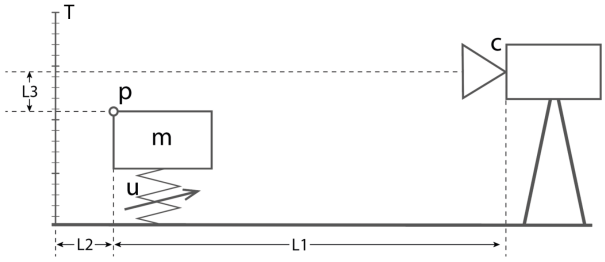

Figure 16: Setup used to measure the dynamic response of the LVDPMGC

With c the camera sensor, u the LVDPMGC, m the isolation mass, p the measurement point, T the measurement tape, and $L1$ to $L3$ the distances between the camera, measurement point and measurement tape. The values for $L1$ to $L3$ are 780mm, 10mm, and 20mm respectively.

The measurement result, shown in figure 17, is obtained by tracking the pixel location of point p and converting the pixel locations to a displacement with the measurement tape. The eigenfrequency is measured at 2.05 Hertz. The damping ratio is determined with the logarithmic decrement formula:

$$\delta = \frac{1}{n} ln(\frac{x_0}{x_n}) \tag{6}$$

With x_0 an extremum of the damped sine wave and x_n an extremum at a number of n cycles later. To get an accurate estimate, the logarithmic decrement formula is used for both maxima and minima and combined to get an average damping ratio of 0.208.

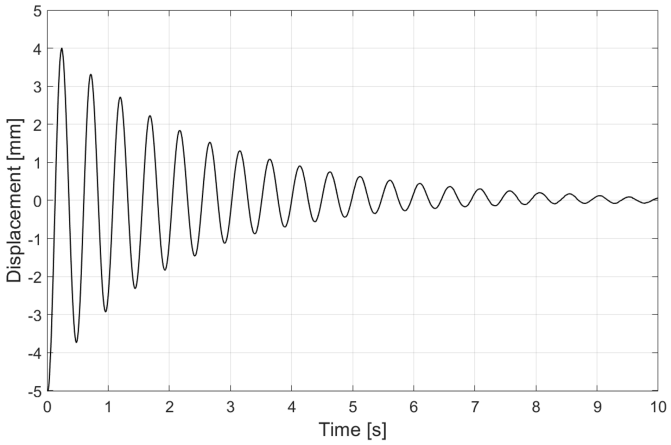

Figure 17: Dynamic response of the LVDPMGC

6 Discussion

This section focuses on the experimental results in more detail. The precision of the measurements and influences on the characteristics of the LVDPMGC are discussed.

To accurately measure the displacement of the unit cell in the dynamic test, the distance between the measurement tape and measurement point p must be considered. Objects at the plane of the measurement point will appear larger because they are closer to the sensor. For small unit cell displacements, this effect is calculated as $(L1 + L2)/L1$. The calibration of the camera is adjusted for this error to obtain accurate results.

A damped sinewave is fitted with the eigenfrequency and damping coefficient found in section 5. To validate these values, the damped sinewave is plotted next to the dynamic measurement in figure 18. The eigenfrequency matches closely throughout the measurement. When looking at the damping coefficient, nonlinear effects start to play a significant role. Since the stiffness of the LVDPMGC over a large range is nonlinear, large vibration amplitudes can behave differently from expectations based on the linear model. After a few periods, nonlinear effects will be smaller due to the lower vibration amplitudes. The determination of the damping coefficient at this timeframe will therefore give a more accurate estimate. When comparing the measurement and the fitted damped sine wave, the measurement shows a slight downward trend. This shows the importance of taking the damping coefficient of both the maxima and minima to reach the average value, as shown in section 5.

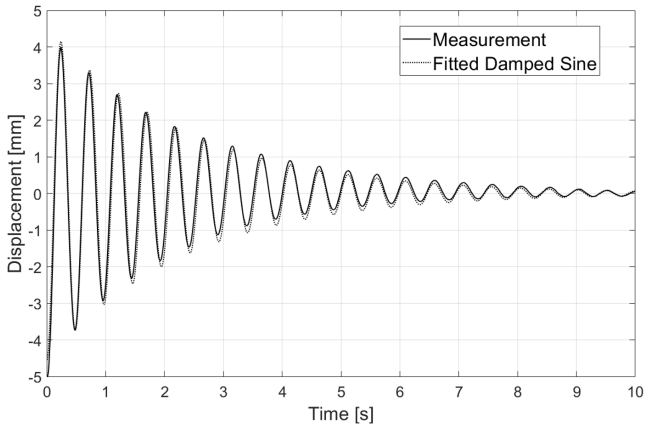

Figure 18: Damped sinewave fit to the dynamic response of the LVDPMGC

The downward trend comes from a phenomenon called creep. It is the tendency of a material to slowly deform under a constant level of stress. While the dynamical test does not induce constant stress in the unit cell, the average loading during the test still causes creep. To measure the amount of creep, a static test is performed with a constant load of 1kg.

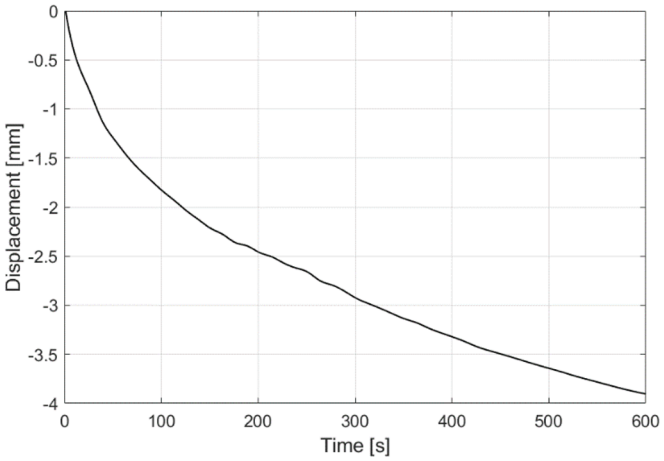

Figure 19: Creep measurements over a time of 600 seconds

Figure 19 shows the results of the creep test. A large displacement of nearly 2mm can be seen in the first 100 seconds. After 100 seconds, the deformation rate goes down and stays relatively constant until the end of the measurement. The large level of creep changes the working point of the unit cell compared to the magnet setup, changing the stiffness of the system. This has a large impact on the performance of the LVDPMGC, decreasing the attenuation range over time. To minimize the effect during the dynamic tests, they are performed quickly after loading.

Other influences on the characteristics of the LVDPMGC can be identified with static tests. The tests are performed in compression and decompression. Figure 20 shows a difference in force between the two measurements. As the measurement speed at 0.1 mm/s was slow, it can be concluded that viscous damping, which is dependent on the frequency of excitation, did not play a major role. Hysteretic damping, caused by the sliding of material layers during increased strain, is not dependent on the frequency of excitation [22], and therefore a likely cause of the force difference. During loading, the sliding of the material layers causes friction, which is dissipated as heat. As energy is lost, the force on decompression is lower.

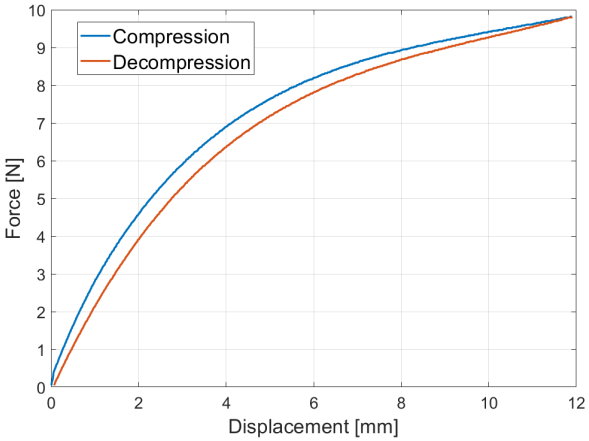

Figure 20: Compression and decompression measurements of the unit cell

Hysteretic damping is dependent on the amplitude of excitation. When attenuating large vibration amplitudes, it can have a significant effect on the high-frequency performance of the LVDPMGC due to the increased damping.

Both Hysteretic damping and creep can be minimized by changing the material. Materials like aluminium exhibit much lower hysteretic damping and creep and can therefore increase performance. As aluminium is a conducting material, eddy current damping will start to play a role. More research on this topic is necessary to understand these effects.

7 Conclusion

This paper focuses on the design of an LVDPMGC for attenuating large-amplitude low-frequency vibrations. The design consists of a unit cell featuring two stepped flexures and a pair of guiding stages, mechanically stabilizing a magnet setup.

Magnet and unit cell simulations were combined, showing the possibility of a high force density and a large range of motion featuring low stiffness. These characteristics can be obtained due to the unit cell exhibiting near equal and opposite stiffness to the magnet setup while exerting a force in the same direction as the magnet setup. The passive stability of the LVDPMGC makes the system easily scalable, creating the possibility of adjusting the load by changing the number of unit cells.

A prototype was manufactured and validated using static and dynamic tests. A large vertical displacement of 7mm with a stiffness below 0.12 N/mm was obtained. Dynamic tests showed a low eigenfrequency of 2.05 Hz with a damping coefficient of 0.208.

Future work will focus on optimizing unit cell dimensions to achieve better performance and implementing different materials in the unit cell to minimize hysteresis and creep.

References

[1] D. L. Platus, "Negative-stiffness-mechanism vibration isolation systems," in *Vibration control in microelectronics, optics, and metrology*, vol. 1619, pp. 44–54, International Society for Optics and Photonics, 1992.

[2] X. Huang, X. Liu, J. Sun, Z. Zhang, and H. Hua, "Vibration isolation characteristics of a nonlinear isolator using euler buckled beam as negative stiffness corrector: a theoretical and experimental study," *Journal of Sound and Vibration*, vol. 333, no. 4, pp. 1132–1148, 2014.

[3] F. Zhao, J. Ji, K. Ye, and Q. Luo, "An innovative quasi-zero stiffness isolator with three pairs of oblique springs," *International Journal of Mechanical Sciences*, vol. 192, p. 106093, 2021.

[4] L. Wu, Y. Wang, Z. Zhai, Y. Yang, D. Krishnaraju, J. Lu, F. Wu, Q. Wang, and H. Jiang, "Mechanical metamaterials for full-band mechanical wave shielding," *Applied Materials Today*, vol. 20, p. 100671, 2020.

[5] H. Fan, L. Yang, Y. Tian, and Z. Wang, "Design of metastructures with quasi-zero dynamic stiffness for vibration isolation," *Composite Structures*, vol. 243, p. 112244, 2020.

[6] C. Cai, J. Zhou, L. Wu, K. Wang, D. Xu, and H. Ouyang, "Design and numerical validation of quasi-zero-stiffness metamaterials for very low-frequency band gaps," *Composite structures*, vol. 236, p. 111862, 2020.

[7] D. M. Correa, T. Klatt, S. Cortes, M. Haberman, D. Kovar, and C. Seepersad, "Negative stiffness honeycombs for recoverable shock isolation," *Rapid Prototyping Journal*, 2015.

[8] T. Zhu, B. Cazzolato, W. Robertson, and A. Zander, "The development of a 6 degree of freedom quasi-zero stiffness maglev vibration isolator with adaptive-passive load support," in *15th International Conference on Mechatronics Technology. URL: http://hdl. handle. net/2440/72548*, 2011.

[9] S. A. J. Hol *et al.*, "Design and optimization of a magnetic gravity compensator," in *4th International Conference of the European Society for Precision Engineering and Nanotechnology*, 2004.

[10] J. Janssen, J. Paulides, E. Lomonova, B. Delinchant, and J.-P. Yonnet, "Design study on a magnetic gravity compensator with unequal magnet arrays," *Mechatronics*, vol. 23, no. 2, pp. 197–203, 2013.

[11] H. Zhang, B. Kou, Y. Zhou, Y. Liu, Q. Ge, and Y. Shao, "Modeling and analysis of a large-load magnetic levitation gravity compensator," in *2019 22nd International Conference on Electrical Machines and Systems (ICEMS)*, pp. 1–5, IEEE, 2019.

[12] T. Zhu, B. Cazzolato, W. S. Robertson, and A. Zander, "Vibration isolation using six degree-of-freedom quasi-zero stiffness magnetic levitation," *Journal of Sound and Vibration*, vol. 358, pp. 48–73, 2015.

[13] H. Zhang, B. Kou, Y. Jin, and H. Zhang, "Modeling and analysis of a new cylindrical magnetic levitation gravity compensator with low stiffness for the 6-dof fine stage," *IEEE Transactions on Industrial Electronics*, vol. 62, no. 6, pp. 3629–3639, 2014.

[14] R. Argiro, "The design and experimental validation of a permanent magnet long-stroke gravity compensator," 2021.

[15] H. Zhang, B. Kou, Y. Jin, H. Zhang, and L. Zhang, "Research on a low stiffness passive magnetic levitation gravity compensation system with opposite stiffness cancellation," *IEEE Transactions on Magnetics*, vol. 50, no. 11, pp. 1–4, 2014.

[16] H. Zhang, B. Kou, and Y. Zhou, "Analysis and design of a novel magnetic levitation gravity compensator with low passive force variation in a large vertical displacement," *IEEE Transactions on Industrial Electronics*, vol. 67, no. 6, pp. 4797–4805, 2019.

[17] D. Xu, Q. Yu, J. Zhou, and S. Bishop, "Theoretical and experimental analyses of a nonlinear magnetic vibration isolator with quasi-zero-stiffness characteristic," *Journal of sound and vibration*, vol. 332, no. 14, pp. 3377–3389, 2013.

[18] S. M. Mofidian and H. Bardaweel, "Theoretical study and experimental identification of elastic-magnetic vibration isolation system," *Journal of Intelligent Material Systems and Structures*, vol. 29, no. 18, pp. 3550–3561, 2018.

[19] G. Dong, X. Zhang, S. Xie, B. Yan, and Y. Luo, "Simulated and experimental studies on a high-static-low-dynamic stiffness isolator using magnetic negative stiffness spring," *Mechanical Systems and Signal Processing*, vol. 86, pp. 188–203, 2017.

[20] R. Berkhof, "Vertical vibration isolation using permanent magnets," 2015.

[21] W. S. P. Robertson, "Modelling and design of magnetic levitation systems for vibration isolation.," 2013.

[22] N. Maia, "Reflections on the hysteretic damping model," *Shock and Vibration*, vol. 16, no. 5, pp. 529–542, 2009.

3 Measurements

In this section, the magnet and unit cell measurements are discussed.

3.1 Magnet Measurements

Magnet dimensions were obtained from the results of early simulations. A measurement setup, shown in figure 3.1, was built to validate the magnet simulations. A force sensor attached to a motion stage measures the force between two magnets. The setup is stabilised by two linear flexure stages, allowing motion along a single axis. The setup is made from plastic and aluminium to minimize any effects on the magnetic field. Measurements are performed horizontally so gravity does not affect the force measurement.

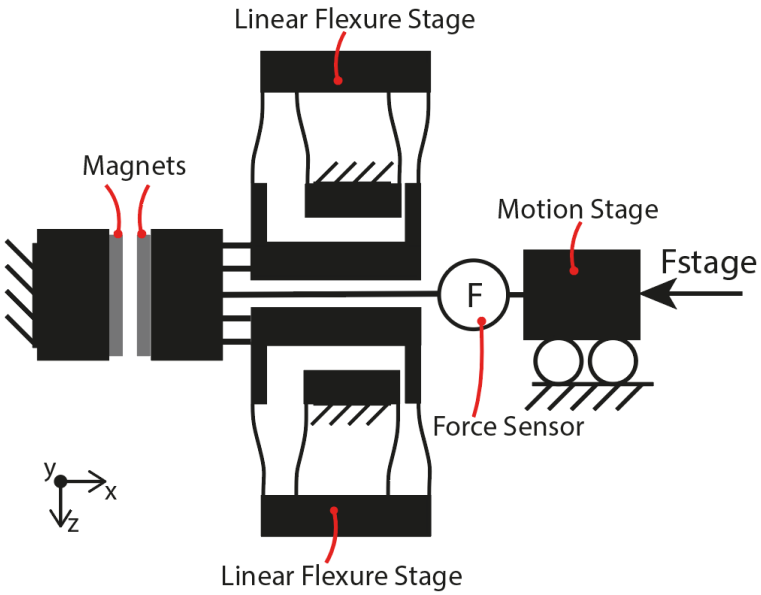

Figure 3.1: Setup to measure the force-displacement characteristics between magnets

To obtain the force between two magnets, two measurements are performed. The first measurement excludes the magnets, measuring the force of the linear flexure stages. The

second measurement includes the magnets, after which the force of the linear flexure stages can be subtracted. This method gives accurate results due to the high repeatability of the flexure stages.

Measurement results are compared to the charge model, introduced in chapter 2 section 3.1. Figure 3.2 shows the results for magnets in attraction. The measurement results are lower than the simulation. This might be due to the manufacturing precision of the magnets, which is shown in appendix A. The maximum fabrication error for the magnet height and depth is stated as 0.1mm while the maximum error for the magnet width is stated as 0.2mm. This can lead to a maximum error of 7.13%. Together with the inaccuracies from the charge model, the results are feasible. Other factors, like the compliance of the measurement setup in x-direction, a possible misalignment of magnets, and the presence of a magnet coating should also be taken into consideration. These factors are small, however, due to the high stiffness of the measurement setup, the automatic aligning of magnets in attraction and a thin coating of only 0.01 mm.

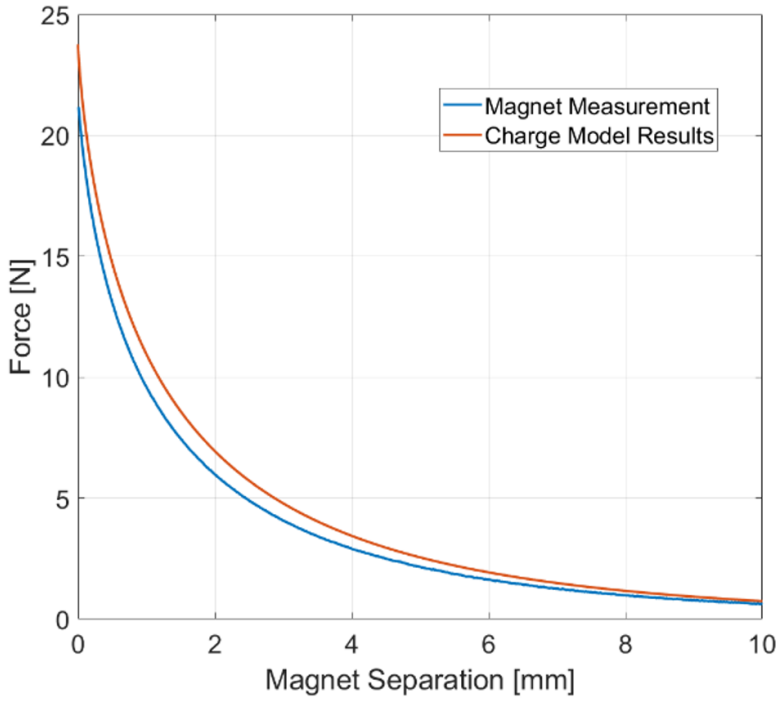

Figure 3.2: Comparison between the magnet measurement and charge model results

3.2 Unit Cell Measurements

The unit cell is measured with the setup shown in figure 3.3. A force sensor attached to a motion stage measures the force of the unit cell. The unit cell is attached to ground and rotated so that gravity has no effect on the force measurement.

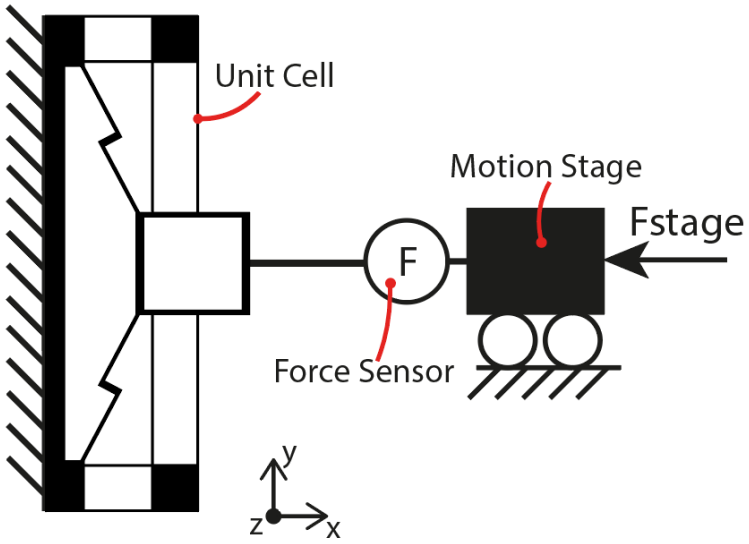

Figure 3.3: Setup to measure the force-displacement characteristics of the unit cell

The force and stiffness results are compared to simulations in figure 3.4. The force characteristics of the measurement are very different from the simulation results. The reasons behind this difference are discussed in chapter 5.2.

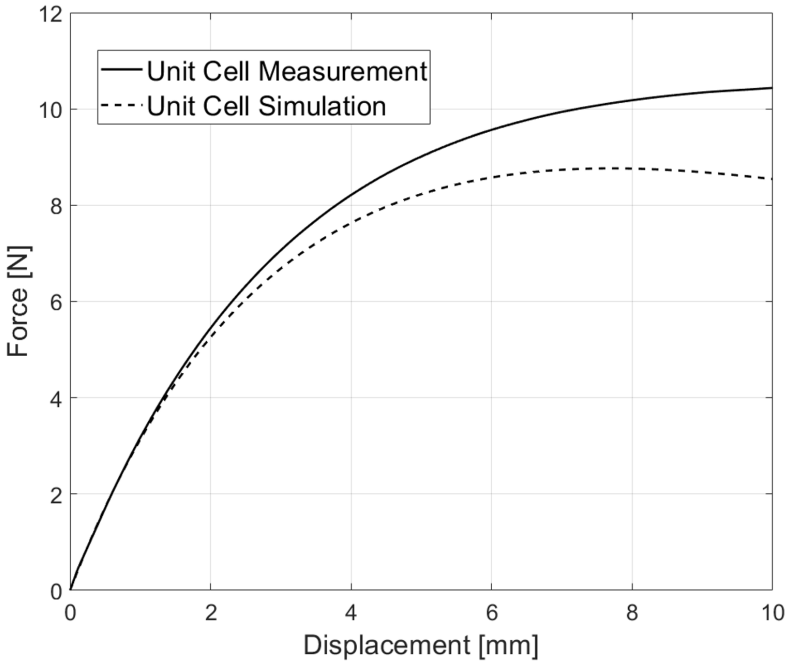

Figure 3.4: Comparison between the force-displacement characteristics of a unit cell measurement and a unit cell simulation

4 Early Design

In this section, an early design is discussed. Its strengths and weaknesses are compared to the final design presented in chapter 2. The early design focuses on stabilizing a magnet setup shown in figure 4.1a. The setup contains two stationary magnets and a moving magnet. The moving magnet, positioned between the stationary magnets, is repelled by the bottom magnet and attracted by the top magnet. A zero-stiffness point is located between a stable and an unstable region. This setup has a large force density, ideal for isolating large loads with a small form-factor. To stabilize this magnet setup, a unit cell shown in figure 4.1b, was designed. It features a positive and negative stiffness region to obtain near opposite stiffness to the magnet setup for a large range of motion.

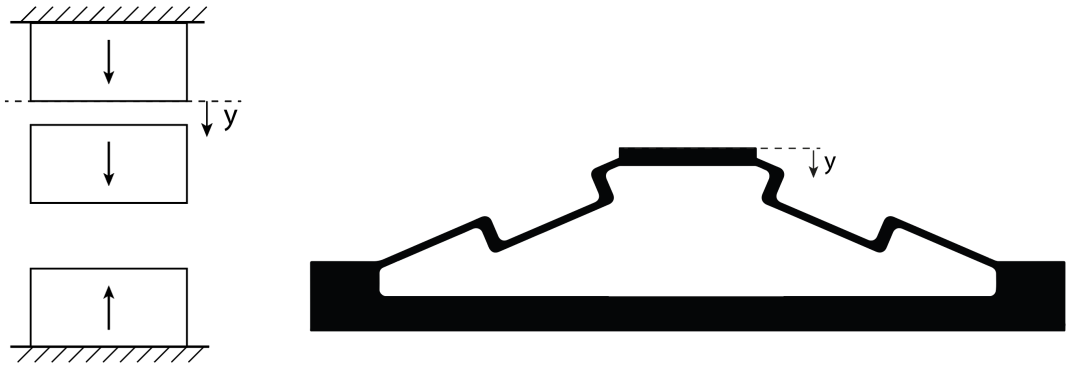

Figure 4.1: a) MGC concept, b) Early unit cell concept

The force characteristics of the unit cell, magnet setup, and their combination are shown in figure 4.2. The design can achieve a stiffness below 0.2 N/mm for a range of 5 mm. A theoretical eigenfrequency of 1.8 Hertz can be obtained.

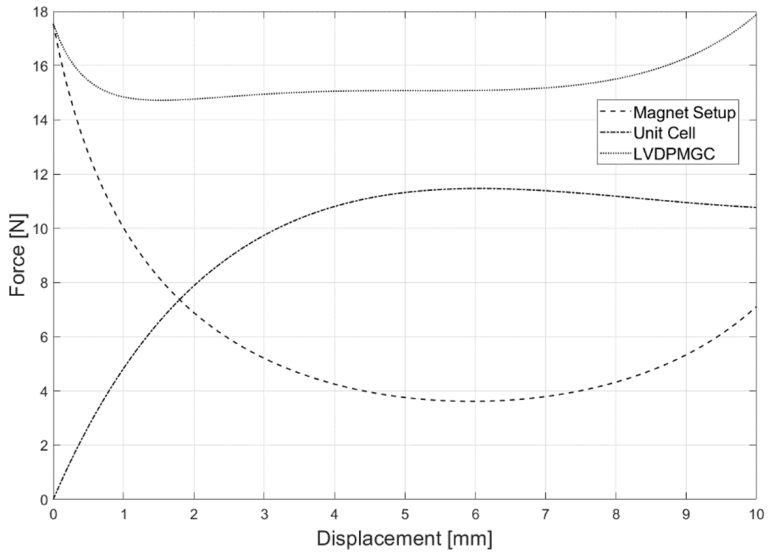

Figure 4.2: force-displacement characteristics of the MGC, unit cell, and their combination

4.1 Magnet Modelling

Early magnet calculations were done with a 2d Finite Element Method (FEM). This method takes the permeability of the magnets into account, increasing modelling accuracy for the magnet setup. As the software calculates the magnets in 2d, the magnetic fields are taken as constant along the length of the model. This introduces a large error when the depth of the magnet is less than 10 times the size of the other dimensions [19]. Since the depth of the magnets in question is not more than 10 times the size of the other dimensions, a 3d COMSOL simulation is used for the calculation of magnet forces. Accurate simulations in 3d take much longer due to the increased number of degrees of freedom. The number of data points is, therefore, minimized to decrease simulation time.

The results of the charge model are compared to the FEM results to see if this analytical method can accurately simulate the magnet setup. Figure 4.3 shows the force and stiffness results of the FEM and charge model. A curve was fitted to the FEM results. While leading to some inaccuracies, it is necessary to create a smooth stiffness plot. It can be seen that the force calculated with the charge model differs slightly from the FEM model. The stiffness characteristics in the area of interest match quite nicely with the FEM results, however. Therefore, the charge model can be used to design a unit cell with opposite stiffness to the magnet setup.

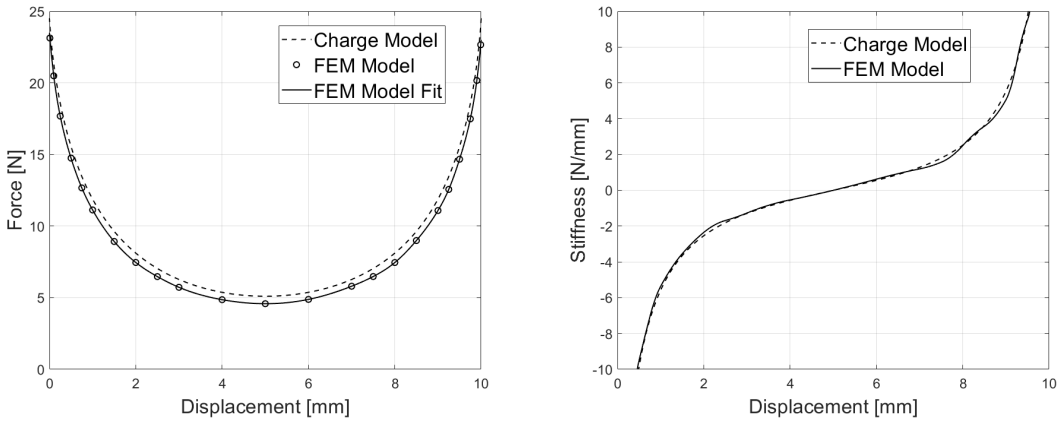

(a) (b)

Figure 4.3: a) Comparison between the MGC force-displacement characteristics of the charge model and a fem model, b) Comparison between the mgc stiffness-displacement characteristics of the charge model and a fem model

4.2 Measurements

The early design requires a measurement for magnets in repulsion and a measurement for magnets in attraction. Results are combined with superposition [20]. The method of superposition can be used to combine multiple magnetic fields when the materials inside the field have a relative permeability of one. Since the magnet permeability is slightly greater than one, an error is induced. This error will be very small because the separation between the stationary magnets is large, and the relative permeability of the magnets is very close to one.

Figure 4.4 shows the measurement results for magnets in repulsion.

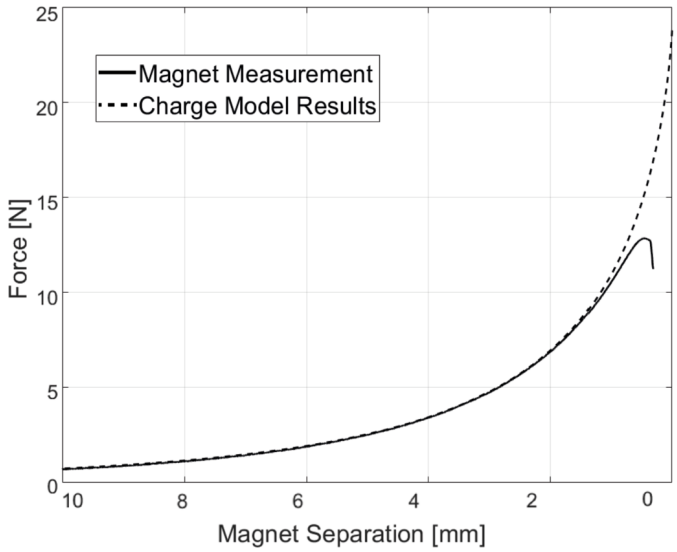

Figure 4.4: Force-displacement characteristics between two magnets in repulsion

Measurements for close magnet separation were hard to obtain owing to the high outward stiffness of the magnets in this range. This caused the linear flexure stages to bend in y-direction, lowering the force between the magnets. Because of this bending, the separation between the magnets was hard to determine. The measurement displacement was therefore fitted to the simulation. Results match nicely for separations larger than 1 mm. When the magnet separation decreases, the measurement force is lower than the charge model result. This can be the result of the permeability of the magnets which causes the field inside the magnet to decrease at close separation. At very close separation, the magnet force goes down due to the bending of the measurement setup. The measurement results from figures 3.2 and 4.4 can be overlapped to create the force plot shown in figure 4.5. Repulsion results were used up to the point where the measurement setup started to bend. The force-displacement characteristics of a setup with a smaller separation of the stationary magnets can be obtained by overlapping a subset of the magnet measurements. This decreases the maximum displacement of the floating magnet but results in a higher overall force.

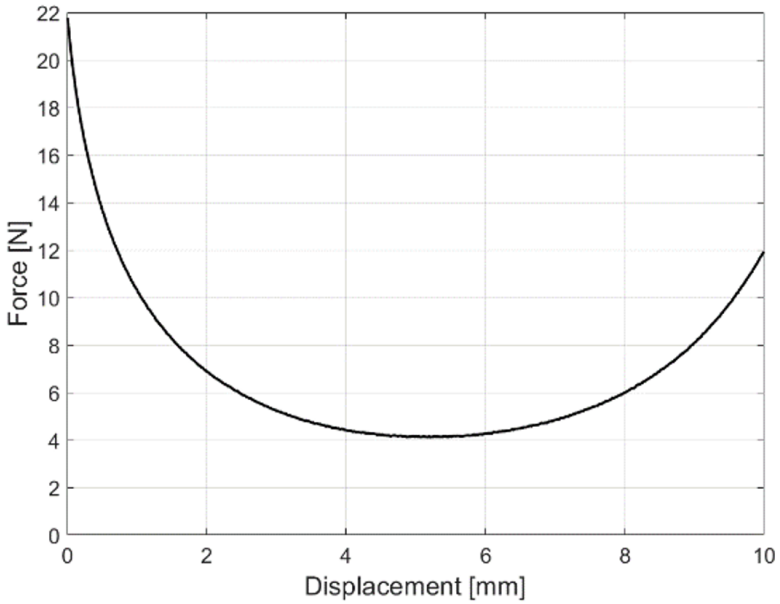

Figure 4.5: Overlapped magnet measurement results for a magnet separation of 11 mm

4.3 Comparison

Strengths of the early design are its high force density and control over the load-bearing capacity by adjusting the separation between the two stationary magnets at the cost of increased stiffness.

The design has multiple weaknesses. The first weakness of the old design comes from rotational instabilities in the mover. These instabilities can be stabilized with a linear motion guiding stage. Such a stage is bulky and works with linear bearings which

introduce friction. An alternative to the linear motion guiding stage is the flexure guiding stage used in the new design. It can be implemented to stabilize the system at the cost of increased stiffness. Both solutions have a negative influence on the system performance. The second weakness of the old design is the tight assembly tolerances necessary for high performance. Assembly errors can have a large influence on the stiffness of the system due to the more complex magnet setup. It is therefore difficult to reach the low theoretical stiffness.
The new design solves the instability and assembly problems. The implementation of the guiding stage helps to obtain opposite stiffness to the new magnet setup while stabilizing the system. The new magnet setup also has fewer parameters which decreases the need for tight assembly tolerances.

5 Fabrication

In this section, the fabrication details of the LVDPMGC are discussed. The prototype was made with Fused Deposition Modelling (FDM). PLA was used as the material for the unit cell. This helped to make quick adjustments to the parameters of the LVDPMGC. A few issues, inherent to FDM technology, arose during prototyping.

5.1 Elephant's Foot

A printing defect called elephant's foot arises when the bottom layers of a print are pushed down by the top layers, causing outward bulging of these layers. Figure 5.1 shows a close-up of the effect.

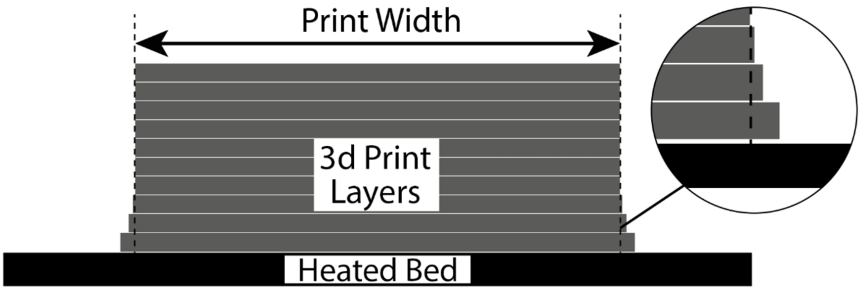

Figure 5.1: Close up of the elephant's foot effect

This outward bulging affects the characteristics of the compliant unit cell. It is important to minimize this effect, which can be done by decreasing the width of the first layers. When the bottom layers start to bulge out, the width of the print equalizes.

5.2 Line Thickness

The dimensions of the unit cell were measured after printing. Small feature sizes were much thicker than modelled, causing unexpected behaviour. This effect was mainly

visible in the guiding stage flexures. They were measured at 0.63mm, where the modelled thickness was 0.45mm. The error originates from the way thin features are handled by the 3d printer. Where a single line of 0.45mm would suffice, the printer passes over the flexure twice. This increases the amount of extruded material and, therefore, the width of the flexures. A new model with adjusted flexure thickness was simulated in COMSOL. The results are shown in figure 5.2. Due to the increased stiffness of the guiding stage, the simulation now matches nicely with the measurement.

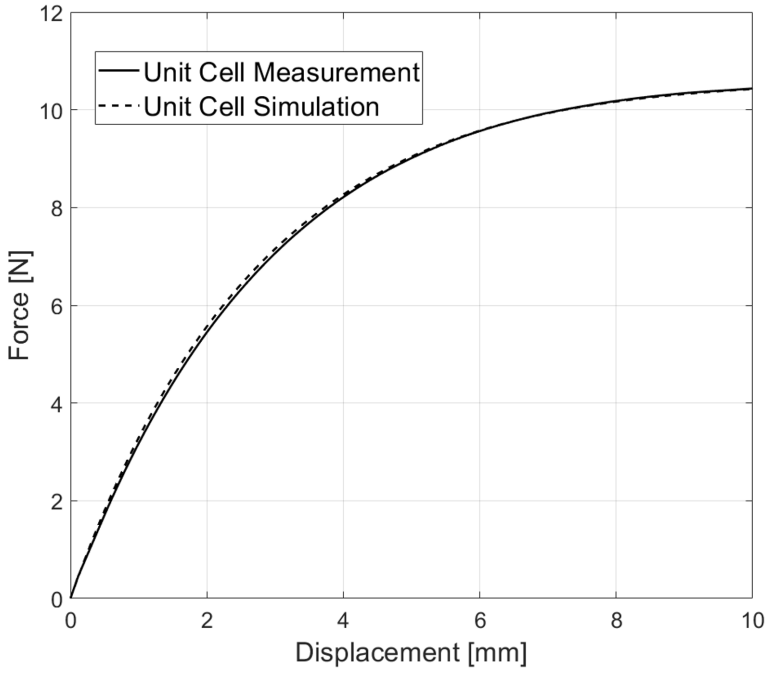

Figure 5.2: Force-displacement characteristic comparison between the LVDPMGC measurements and LVDPMGC simulation results with adjusted flexure width

6 Performance Evaluation

This chapter discusses the performance of the LVDPMGC. The stability of the LVDPMGC is analysed and its nonlinear behaviour is dynamically modelled.

6.1 Unit Cell Stability

The unit cell stiffness in translation and rotation is simulated to get a better understanding of the system stability. Figure 6.1 shows the axis orientation of the unit cell. Throughout the working range of the LVDPMGC, the stiffness of the magnet setup is more than two orders smaller than the unit cell and is therefore not considered.

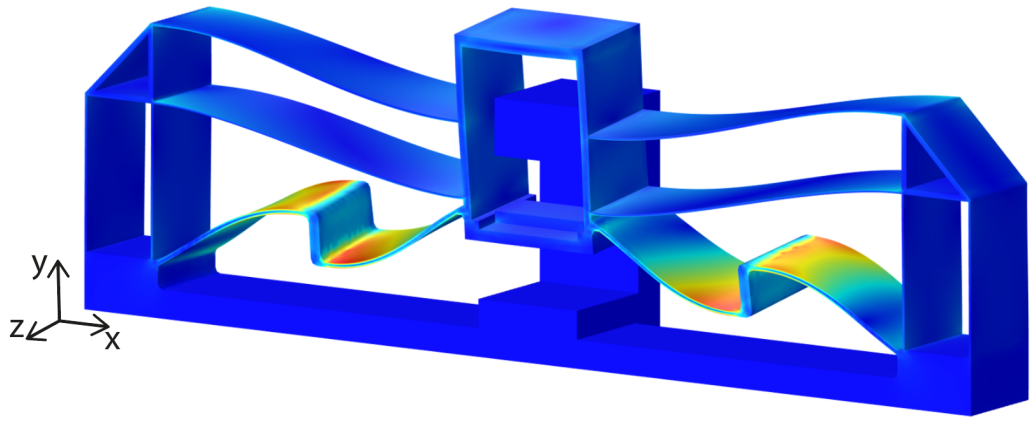

Figure 6.1: COMSOL simulation for an applied moment to the top of the unit cell

Figure 6.2 shows the translational and rotational stiffness of the unit cell for varying displacement.

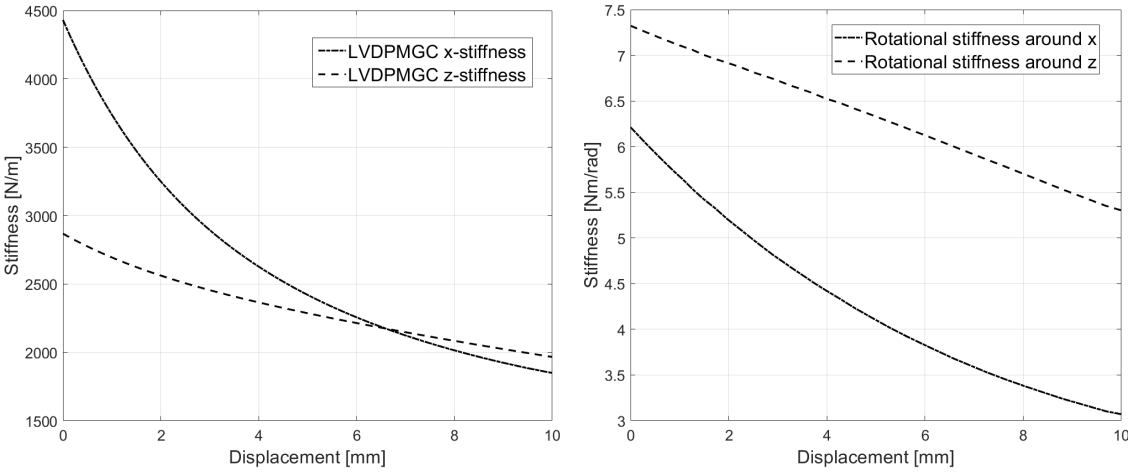

(a) (b)

Figure 6.2: a) Unit cell stiffness in translation for varying displacement, b) Unit cell stiffness in rotation for varying displacement

Figure 6.2a shows a strong decline in x-stiffness for increasing displacement. This is because the stepped flexures, which offer most of the stiffness in this direction, slowly buckle at increasing displacement which significantly reduces their stiffness. The z-stiffness is less affected by the displacement.
The translational stiffness of the LVDPMGC makes the system unfit to isolate vibrations in these directions. Horizontal vibrations are, however, much easier to attenuate because the direction of the load and the direction of vibrations are different. An example of a horizontal isolator is discussed in [2]. Figure 6.3 shows an adjusted version of this horizontal isolator. It consists of four wire flexures which are rigidly connected to the ground and to the isolation mass, leaving the system unconstrained in planar motion. When the mass is increased to the buckling load of the wire flexures, the system reaches zero stiffness in the horizontal plane. Such an isolator can effectively attenuate vibrations in the horizontal plane.

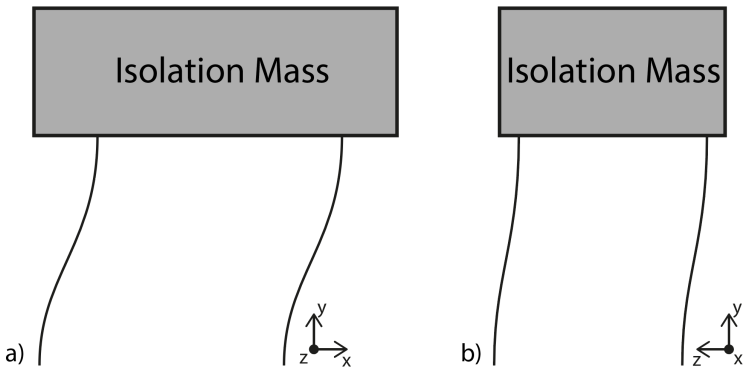

Figure 6.3: Schematic of a horizontal isolator adapted from [2], a) front view, b) side view

The rotational stiffness, shown in figure 6.2b, is determined by putting a moment on the top of the unit cell. The stiffness around x decreases quickly at increasing displacement. This is because the stepped flexures quickly lose rotational stiffness in their buckled state. The stiffness around z does not decrease as much because the guiding stage, which offers most of the stiffness in this direction, is less affected by an increase in displacement.

Due to the limited stiffness around x and y, a shift in the isolation mass will result in a rotation of the unit cell. This can change the characteristics of both the magnets and the unit cell. It is therefore important to place the centre of gravity of the isolation mass in the middle of the unit cell.

6.2 Nonlinear Model

A nonlinear model of the LVDPMGC is created with the static measurement results from chapter 2 section 5. The LVDPMGC is modelled as a nonlinear spring, u in parallel with a damper c, shown in figure 6.4. The system is excited by a chirp signal, x_c, which causes a displacement of the mass, x_m.

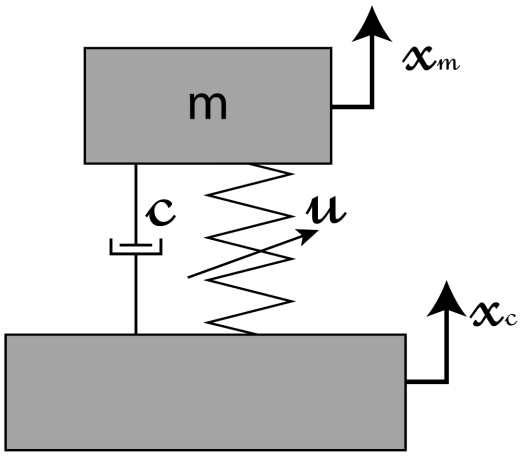

Figure 6.4: Schematic representation of the LVDPMGC

The transmissibility function of the system can now be found by dividing the oscillation of the mass by the chirp signal in the frequency domain. The transmissibility function for two chirp signals with different amplitudes is given in figure 6.5. The nonlinearity in the system causes a slight shift in eigenfrequency and peak amplitude. The difference is, however, very small. This indicates that there is only a very low level of nonlinearity in the system.

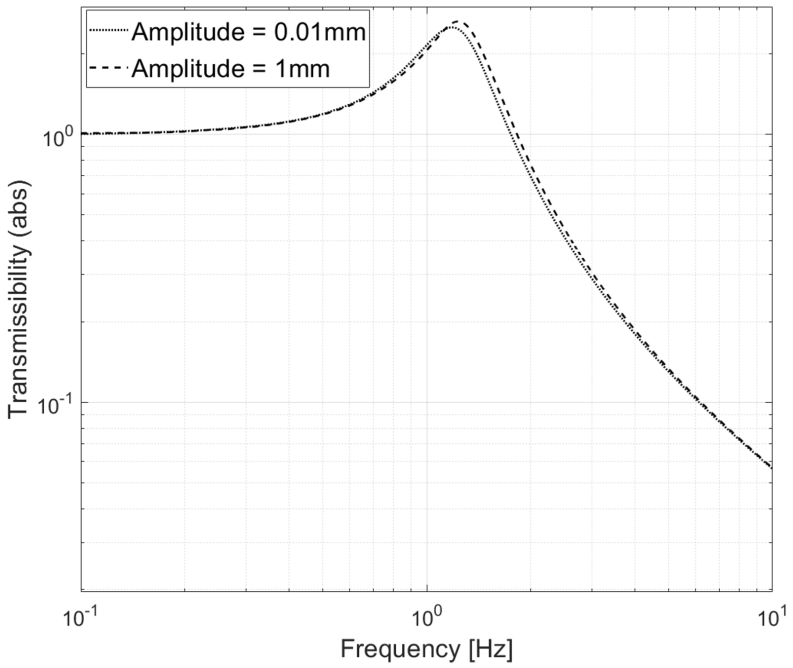

Figure 6.5: Transmissibility of the LVDPMGC for multiple vibrational amplitudes

The transmissibility of the LVDPMGC is compared to the transmissibility of the designs from Berkhof et al. [14] and Platus et al. [2]. While both designs have a lower eigenfrequency, the design of Berkhof et al. has a significantly higher damping ratio, which makes the system perform poorly at higher vibration amplitudes. The design by Platus et al. outperforms the LVDPMGC. It is, however, much more complex while the LVDPMGC features only three parts.

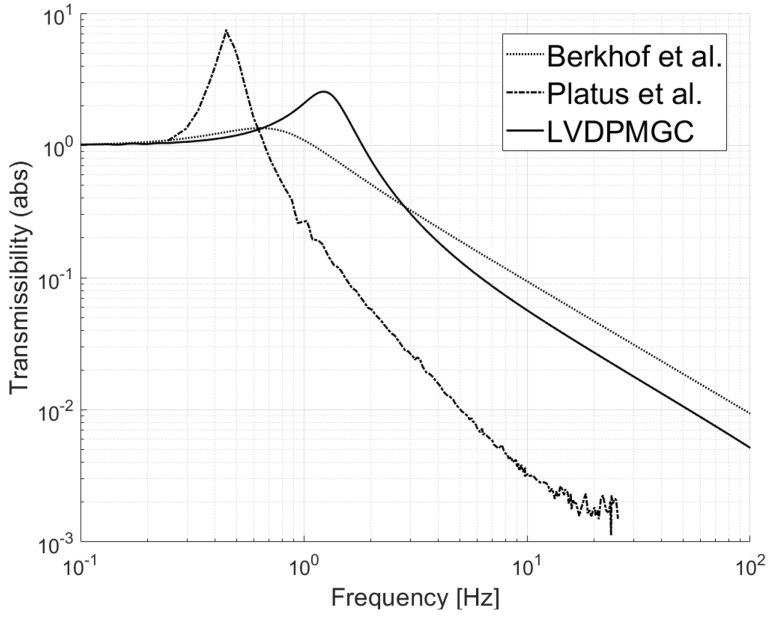

Figure 6.6: Transmissibility comparison between vibration isolators from literature

7 Discussion

This chapter focuses on details of the results and limitations in the evaluation methods from chapter 6.

- The rotational stiffness of the unit cell is determined by placing a moment on the top of the unit cell. The centre of rotation of the unit cell lies close to the mover magnet, at which the unit cell has a different rotational stiffness. The exact centre of rotation is, however, hard to determine because it changes from where the unit cell is loaded.
- Besides the importance of proper load placing, the low rotational stiffness can also lead to unwanted vibrations. When a load is placed on the unit cell, horizontal vibrations can cause the unit cell to start vibrating around x or z. This is due to the centre of gravity of the load being above the centre of rotation of the unit cell, resulting in a moment when the mass accelerates. To minimize this effect, the centre of gravity must not be too high.
- The nonlinear model does not consider higher-order modes of the system. These can include the vibration of individual flexures which can have a negative effect on the transmissibility of the system.
- Creep and hysteresis are not considered in the nonlinear model due to the difficulty of modelling these effects. They have a large impact on the performance of the LVDPMGC which changes the real-world characteristics compared to the nonlinear model.

8 Conclusion and Recommendations

8.1 Conclusion

This research aims to answer the following research question:

"How can a nonlinear stiffness unit cell stabilize a long stroke magnetic gravity compensator while increasing its range of motion and scalability?"

The research question is answered by completing three sub-objectives. First, a magnet setup is chosen by analysing the parameters of interest for both the magnets and the unit cell. The parameter analysis shows the importance of the magnet aspect ratio to obtain compatible force-displacement characteristics between the magnet setup and unit cell.
Second, the parameters of the unit cell are iteratively adjusted to oppose the stiffness of the magnet setup. A set of design objectives is composed to evaluate the performance of the LVDPMGC. A prototype is fabricated which passes all design requirements.
Third, the prototype is validated using static and dynamic tests. A large vertical displacement of 7mm with a stiffness below 0.12 N/mm is obtained while maintaining passive stability. This passive stability increases the scalability of the system, creating the possibility of changing the isolation mass by increasing the number of unit cells in the system. Dynamic tests show a low eigenfrequency of 2.05 Hz with a damping coefficient of 0.208.
Together, the sub-objectives answer the research question, showing how a nonlinear stiffness unit cell can stabilize a long-stroke magnetic gravity compensator while increasing its range of motion and scalability.

8.2 Recommendations

This section summarizes recommendations for future research.

- The parameters of the LVDPMGC can be optimized. Where current parameters were iteratively adjusted, an optimization process could lead to much higher performance.
- A change of flexure material should be considered to minimize creep and hysteresis, but also damping in the system, increasing high-frequency performance. A material like aluminium can decrease creep, hysteresis, and material damping, but due to its high conductivity eddy current damping will start to play a role. Titanium, a poor conductor, will show much less eddy current damping, but will significantly increase the cost of the system. More research will be necessary to find an optimal flexure material, obtaining high performance at low-cost.
- A fatigue analysis of the unit cell should be performed to see if the dynamic loading of the flexures causes any degradation in the material over time.
- To get a more accurate transmissibility plot, a dynamic measurement of the LVDP-MGC should be performed. The setup for this includes a low-frequency shaker and device to measure the output position of the LVDPMGC like a laser interferometer or a high-speed camera.
- To increase the force density of the magnet setup, an alternating magnet array could be implemented in the stator and mover. In such a design a magnet has opposite polarization to its neighbours, creating an array of magnets. This magnet array creates a more defined flux path for the magnetic field. Another option is to replace both the mover and stator magnets with a Halbach array. Such an array increases the magnetic field on one side of the magnets while decreasing the magnetic field on the other side of the magnets. This could increase the force density of the design and minimize the magnetic field where it is not wanted. More research is necessary to find the force characteristics between two Halbach arrays and possible risks like demagnetization.
- To minimize disturbing sensitive equipment with the magnetic field created by the magnet setup, magnetic shielding could be implemented. The effect of this shielding on the force-displacement characteristics of the magnet setup should be researched.
- The adjustable load-bearing capacity of the early design can be very interesting for implementing multiple unit cells in a lattice design to make a metamaterial. The adjustable load-bearing capacity is necessary for a vertically stacked lattice because the bottom unit cells carry the weight of the load and the top unit cells whereas the top unit cells only carry the load. Such a metamaterial can create a lower eigenfrequency or frequency bandgaps, as discussed in [7].

A Datasheet of the magnets used in the LVDPMGC prototype

Please refer in correspondence: HKCM-Drawing number 9964-53824

QR-CODE

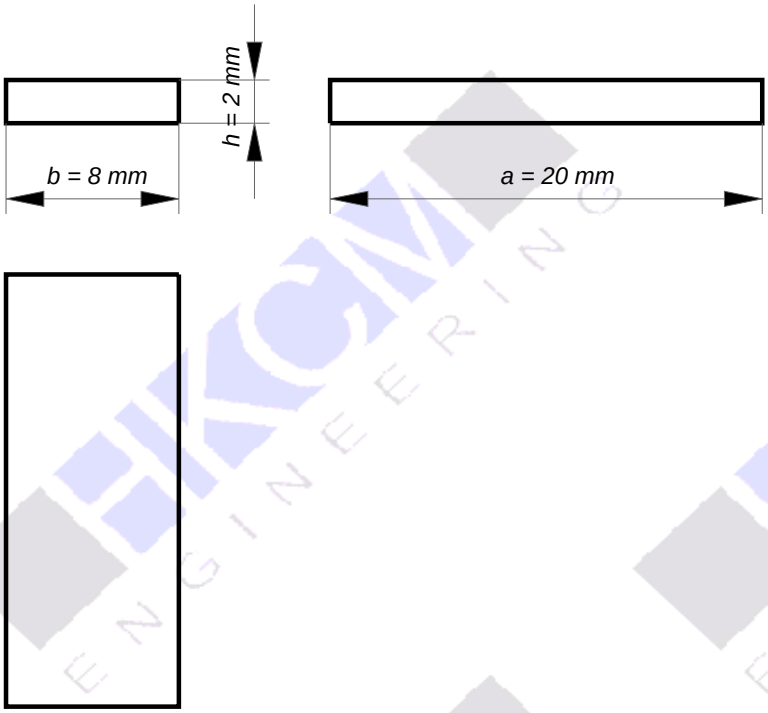

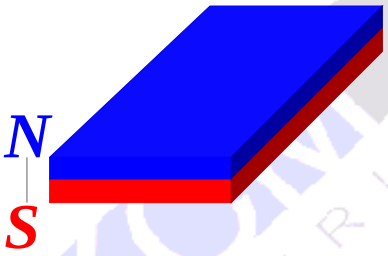

Magnet-Cuboid Q20x08x02Ni-N35

Tolerances : DIN ISO 2768-1m (Website Download Center)
ROHs (2011/65/EU) & REACh (2007/EU)
Length(a) = 20 mm ()
Width(b) = 8 mm ()
Height(H) = 2 mm ()
Material/grade: NdFeB / N35
Coating: Nickel
max.operation temperature = 80°C
Flux density inside the magnet = 1.17 Tesla
Temperature coefficient and flux = 0.11% per 1°K
Dead weight: 2.389 g
Holding force on iron 13.83 Newton
Weight, which the magnet can lift: 1.41 kg

HKCM Engineering e.K.
Ottestr.20
D-24340 Eckernfoerde
tel: +49 (0) 4351 726 461
fax: +49 (0) 4351 726 463
mail: sales@hkcm.de
web: https://www.hkcm.de
MwSt./VAT-Id No.: DE 814 756 521

Tolerances and limits

If not stated otherwise in the respective HKCM drawings our magnets are manufactured according to DIN ISO 2768-1m. The drawings are generated automatically based on the data in our system.

Additional standards
DIN EN ISO 286-1: A basis for tolerances, permissible allowances and fitting tolerances
DIN EN 60404-5: Magnetic materials - Procedures for measurement of magnetic properties

Limits for lenghts, diameters, angles and radius on blocks, cylinders, rings, segments, loafs, trapezoids and spheres

Base measurement	0.5 - 3 mm	>3 - 6 mm	>6 - 30 mm	>30 - 120 mm	>120 mm
D/d/l/w/h -/+	0.1 mm	0.1 mm	0.2 mm	0.3 mm	0.5 mm
Edge roundings)	0.2 mm	0.5 mm	1.0 mm	2.0 mm	4.0 mm
Angle -/+	1°	1°	30 '	20 '	10 '

The permissible deviation of the magnetic field strength at a 0 mm distance is -/+ 10%. It should be taken into consideration that the outside and measurable flux density of the magnetic field is just 1/3 of the inside flux density of the magnet.

The permissible deviation of the field direction from the symmetrical axis at a 2 mm distance is -/+ 10%. This does not apply for other positions. It is impossible to reach a homogeneous magnetic field in practical conditions due to a multiplied chaining of tolerances.

Therefore measuring and adjusting the fitting position and that of the relevant components (Hall, Reed) in their surroundings (ferritic materials) is a pre-condition for using permanent magnets for sensoring purposes.

The max. permissible operating temperature given for each type of magnet should only be reached for a short period. The same applies for temperatures reached at certain mounting and fitting procedures (casting, bonding, soldering). Permanently Neodymium and Samarium-Cobalt magnets should only be used at 2/3 of their max. operating temperature.

HKCM Engineering e.K.
Ottestr.20
D-24340 Eckernfoerde
tel: +49 (0) 4351 726 461
fax: +49 (0) 4351 726 463
mail: sales@hkcm.de
web: https://www.hkcm.de
MwSt./VAT-Id No.: DE 814 756 521

Area of application for material & coating

Area of application for the coating

Parylene 	<0.05mm Pc, polymere applied in vaccum chamber, optically opaque, surface beneath visible	best none metallic protection against corrosion, hydrophobe, watertight & gastight, non-soluble, barrier against organic & anorganic substances, strong acids & alkaline solution, gas & steam, structure-preserving, low friction coefficient, di-electric, meets MIL-I-46058C, non-toxic, fungus & bacteria tight, bio-compatible, physiologically & toxicologically harmless, anti-allergic
Teflon 	>0.02mm NiTf, plastic layer, blue, soft and elastic surface	good protection against corrosion, water-repellent, barrier against organic & anorganic substances, strong acids & alkaline solution, gas & steam, structure-preserving, low friction coefficient, di-electric, mechanically sensitive
Epoxy 	>0.05mm Ep, plastic layer in dip-coating process, black, soft and elastic surface	good protection against corrosion, water-repellent, mechanically sensitive
Gold 	>0.01mm Ni+Cu+Ni+Au, galvanically applied golden surface, Industry-Gold or 24Karat	best metallic protection against corrosion, very good electrical conductivity, no negative effect at body contact
Silver 	>0.01mm Ni+Cu+Ni+Ag, galvanically applied silver, soft surface	very good protection against corrosion, very good electrical conductivity, typical black oxid can be removed with cleaning cloth, no negative effect at body contact, pay attention to the right magnet material (max.op.temp.) if soldering is planned
Tin 	>0.01mm Sn, galvanically applied silver, soft and tight surface	very good protection against corrosion, good electrical conductivity, no negative effect at body contact, pay attention to the right magnet material (max.op.temp.) if soldering is planned
Chrome 	>0.01mm Ni+Cu+Ni+Cr, galvanically applied dark silver-like, tight and hard surface	very good protection against corrosion
Zinc 	>0.006mm Zn, galvanically applied blue silver-like, tight and even surface	good protection against corrosion
Nickel 	**>0.01mm Ni+Cu+Ni, galvanically applied silver or dark silver-like, porose and hard surface**	**Industrial standard, good work stability, sufficient protection against corrosion in dry ambients, possible allergic reaction on sensible persons**
not coated 	Magnet material grey metallic	acceptable for SamariumCobalt - but no good mechanical protection, not acceptable for Neodymium - oxidation in wet ambients, dissolution in acids, lightly resistant in alkaline suspensions. Sealing neccessary.

N	N35	M	H	SH	UH	EH	YX	YXG	FCC
60°C 140°F	**80°C 176°F**	100°C 212°F	120°C 248°F	150°C 302°F	180°C 356°F	200°C 392°F	250°C 482°F	350°C 662°F	500°C 932°F

*)

- Iron Chrome Cobalt (FeCrCo), soft magnetic, machinable
- Samarium Cobalt Sm2Co17, very brittle, not machinable
- Samarium Cobalt Sm2Co5, brittle, not machinable
- Sintered Neodymium, very strong & hard, not machinable
- Bonded magnets, machinable

HKCM Engineering e.K.
Ottestr.20
D-24340 Eckernfoerde
tel: +49 (0) 4351 726 461
fax: +49 (0) 4351 726 463
mail: sales@hkcm.de
web: https://www.hkcm.de
MwSt./VAT-Id No.: DE 814 756 521

Magnet-Cuboid Q20x08x02Ni-N35

ROHs (2011/65/EU) & REACh (2007/EU)
Material/grade: NdFeB / N35 / 279kJ/m3
Coating: Nickel
max.operation temperature = 80°C
Temperature coefficient and flux = 0.11% per 1°K

Area of application for material & coating

Properties Neodymium (NdFeB)

Neodymium is the strongest magnet material available.
It has up to 1.43 Tesla and can resist up to 200°C depending on the specification.
Neodymium is very hard and brittle. It is nearly impossible to machine it.
Neodym magnets are manufactured from rare powder materials under high pressure and are then coated with thin metal layers.
The material is brittle and can easily break or be damaged on the surface when two or more magnets come in contact.
The basic material can create sparks through contact, and sparking may ignite.
Mostly these magnets are covered with a metallic coating which does not protect against corrosion in humid conditions.
Parylene coating is the only efficient protection.

HKCM Engineering e.K.
Ottestr.20
D-24340 Eckernfoerde
tel: +49 (0) 4351 726 461
fax: +49 (0) 4351 726 463
mail: sales@hkcm.de
web: https://www.hkcm.de
MwSt./VAT-Id No.: DE 814 756 521

Magnet-Cuboid Q20x08x02Ni-N35

ROHs (2011/65/EU) & REACh (2007/EU)
Material/grade: NdFeB / N35 / 279kJ/m3
Coating: Nickel
max.operation temperature = 80°C
Temperature coefficient and flux = 0.11% per 1°K

NdFeB, N35 - IEC 260/95

This diagram is based on the extensive data collection of HKCM Engineering e.K. It is a representative example for magnets made of material with grade CGS N35 / IEC 260/95

The y axis gives values of the magnetic flux density B in the magnet and the magnetic polarisation J.

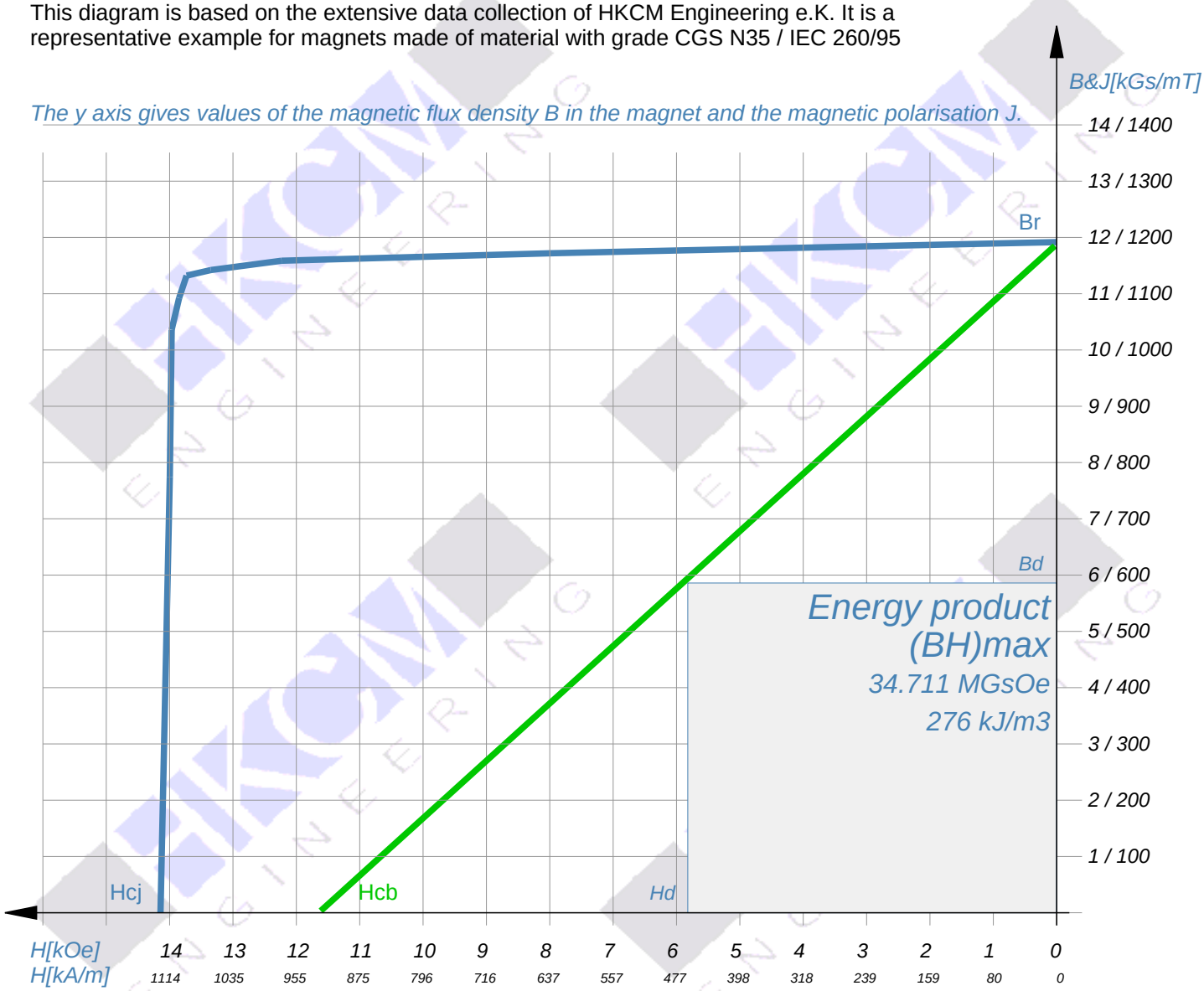

The x axis shows the values of the externally applied coercitive field strength H.

The energy product is the largest possible rectangular area below the Br/Hcb curve
acc. to official SI-standard (based on IEC 60404-8-1): (BH)max = Vs/m2 * A/m = [kJ/m3]
acc. to CGS-standard (common use): (BH)max = (BH)max = kGauss * kOersted = [MGsOe]
These figures are used for the description and identification of the grade of magnets.

Magnet-Cuboid Q20x08x02Ni-N35

Energy product	(BH)max	34.711 MGsOe	276 kJ/m3
Flux density	Br	11.917 kGs	1192 mT / 1.19 Vs/m2
	Bd	5.9095 kGs	591 mT / 0.59 Vs/m2
	Hcb	11.625 kOe	925 kA/m
	Hcj	14.144 kOe	1126 kA/m
	Hk	13.854 kOe	1102 kA/m
	Hk/Hcj	97.9 %	97.9 %
	Hd	5.8737 kOe	467 kA/m
max.operation temperature = 80°C			
Temperature coefficient and flux = 0.11% per 1°K			

HKCM Engineering e.K.
Ottestr.20
D-24340 Eckernfoerde
tel: +49 (0) 4351 726 461
fax: +49 (0) 4351 726 463
mail: sales@hkcm.de
web: https://www.hkcm.de
MwSt./VAT-Id No.: DE 814 756 521

Force at a distance s

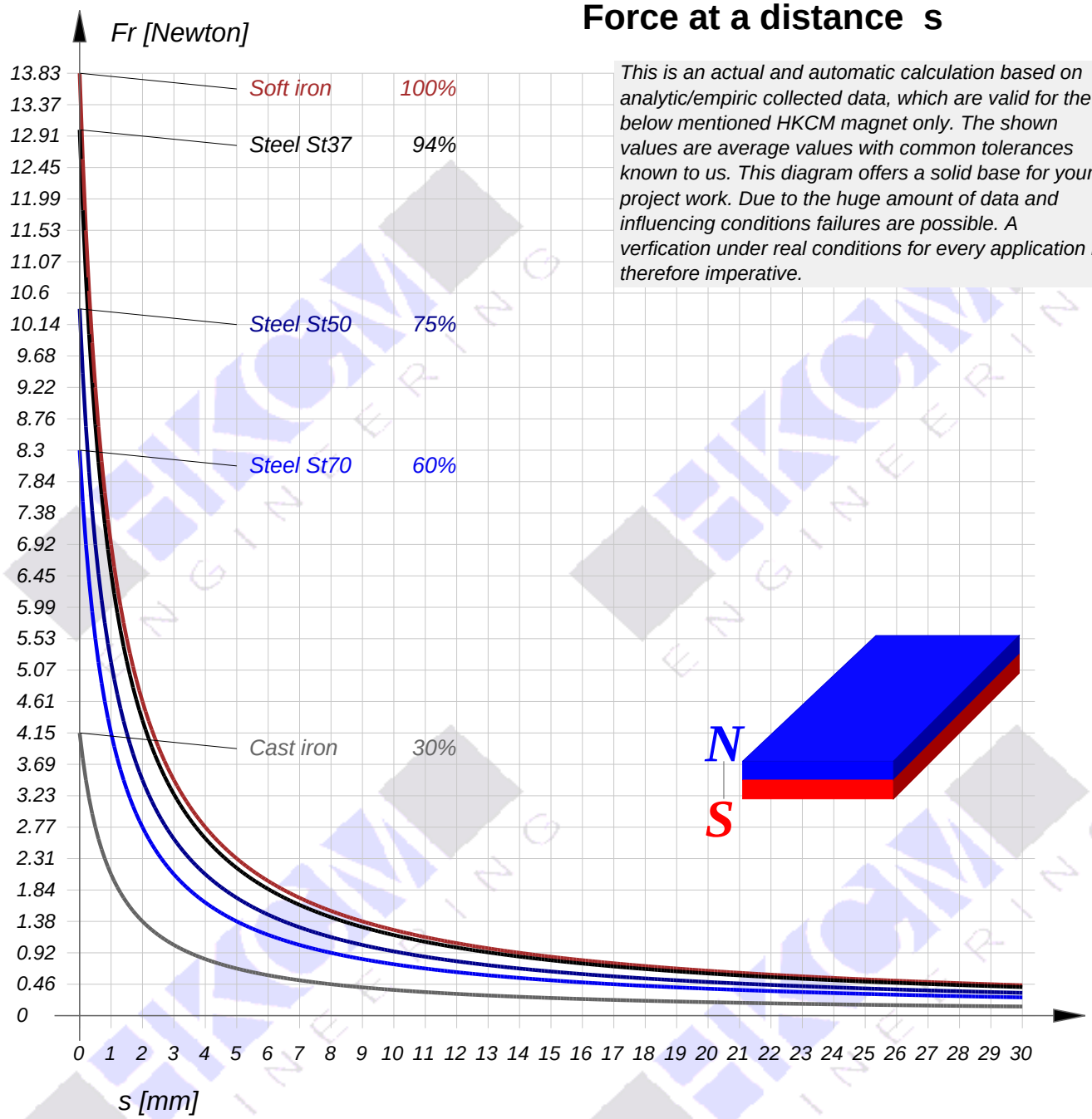

This is an actual and automatic calculation based on analytic/empiric collected data, which are valid for the below mentioned HKCM magnet only. The shown values are average values with common tolerances known to us. This diagram offers a solid base for your project work. Due to the huge amount of data and influencing conditions failures are possible. A verfication under real conditions for every application is therefore imperative.

Magnet-Cuboid Q20x08x02Ni-N35

Tolerances : DIN ISO 2768-1m (Website Download Center)
ROHs (2011/65/EU) & REACh (2007/EU)
Length(a) = 20 mm ()
Width(b) = 8 mm ()
Height(H) = 2 mm ()
Material/grade: NdFeB / N35
Coating: Nickel
max.operation temperature = 80°C
Flux density inside the magnet = 1.17 Tesla
Temperature coefficient and flux = 0.11% per 1°K
Dead weight: 2.389 g
Holding force on iron 13.83 Newton
Weight, which the magnet can lift: 1.41 kg

HKCM Engineering e.K.
Ottestr.20
D-24340 Eckernfoerde
tel: +49 (0) 4351 726 461
fax: +49 (0) 4351 726 463
mail: sales@hkcm.de
web: https://www.hkcm.de
MwSt./VAT-Id No.: DE 814 756 521

Measurement of the magnetic force

The measurement of the magnetic force is a technical challenge if there is no suitable measurement system available (e.g. test machine Houndsfield HTE).

With the help of test equipment and assisting measures in a workshop an estimate can be determined but no exact and verifiable measurement. The magnetic characteristics, volume and form of the magnet and the ambient conditions are decisive for the force leading to an attraction of ferruginous material. The resulting magnetic force probably comes from its centre of mass. To get an exact measurement the magnet should be hanged on a cardan suspension at this centre of mass to eliminate any other force directions and shearing strength. This is virtually impossible.

For a makeshift measuring equipment at least a calibrated spring balance, a counterpart made of pure iron and a cardan suspension for magnet and counterpart are necessary. Any other ferruginous items or magnets must be kept away from the measuring set.

Common mistakes:

- ferruginous material in the vicinity
- characteristics of the counterpart (e.g. wrong size, quality, geometry, rough surface)
- air gaps (e.g. dirt, paint, coats or other distancing matters)
- shear forces e.g. made by wrong set installation, tension by wrong clamping or locking
- damages on the magnet or counterpart (mechanical or corrosive)
- disregard of the temperature (21°C)

Typical deviations at magnet measurements result from technical characteristics of magnets (graininess, dimensions, surface, magnetization) and their interaction with the ambient situation. Measuring tolerances should be considered as multiplicatively as with any other technical articles.

The values given in our data sheets are based on current and automatic calculations with the help of analytically and empirically captured data. The values given are means in view of tolerances from practical work and as such form a solid basis for your planning. Errors cannot be ruled out based on the amount of various influences and data. A verification in practice is a matter of urgent necessity.

HKCM ENGINEERING

HKCM Engineering e.K.
Ottestr.20
D-24340 Eckernfoerde
tel: +49 (0) 4351 726 461
fax: +49 (0) 4351 726 463
mail: sales@hkcm.de
web: https://www.hkcm.de
MwSt./VAT-Id No.: DE 814 756 521

Flux at a distance s

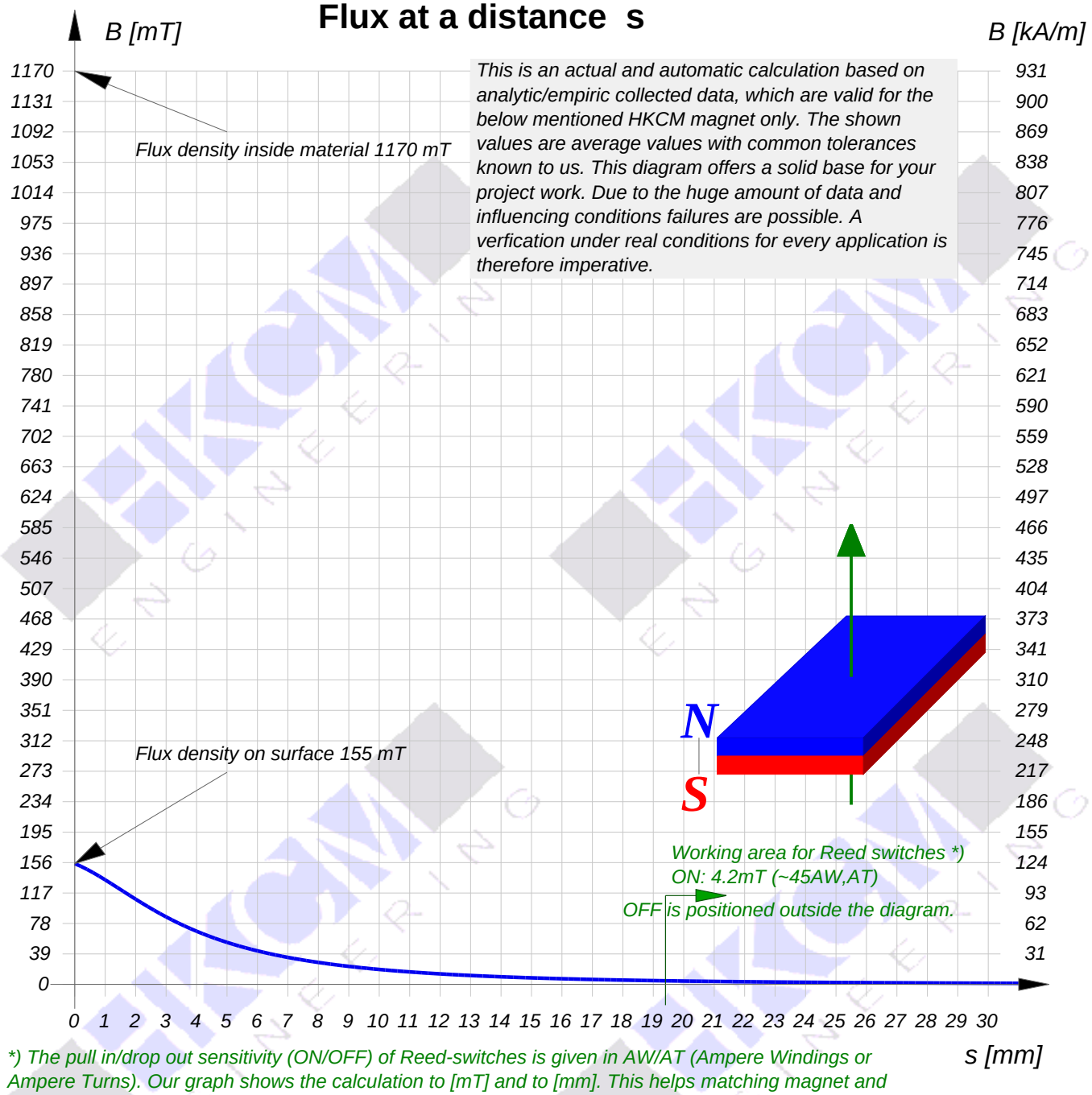

*) The pull in/drop out sensitivity (ON/OFF) of Reed-switches is given in AW/AT (Ampere Windings or Ampere Turns). Our graph shows the calculation to [mT] and to [mm]. This helps matching magnet and switch.

Magnet-Cuboid Q20x08x02Ni-N35

Tolerances : DIN ISO 2768-1m (Website Download Center)
ROHs (2011/65/EU) & REACh (2007/EU)
Length(a) = 20 mm ()
Width(b) = 8 mm ()
Height(H) = 2 mm ()
Material/grade: NdFeB / N35
Coating: Nickel
max.operation temperature = 80°C
Flux density inside the magnet = 1.17 Tesla
Temperature coefficient and flux = 0.11% per 1°K
Dead weight: 2.389 g
Holding force on iron 13.83 Newton
Weight, which the magnet can lift: 1.41 kg

HKCM Engineering e.K.
Ottestr.20
D-24340 Eckernfoerde
tel: +49 (0) 4351 726 461
fax: +49 (0) 4351 726 463
mail: sales@hkcm.de
web: https://www.hkcm.de
MwSt./VAT-Id No.: DE 814 756 521

Bibliography

[1] G. W. van der Poel, "An exploration of active hard mount vibration isolation for precision equipment," *Ph. D. thesis*, 2010.

[2] D. L. Platus, "Negative-stiffness-mechanism vibration isolation systems," in *Vibration control in microelectronics, optics, and metrology*, vol. 1619, pp. 44–54, International Society for Optics and Photonics, 1992.

[3] X. Huang, X. Liu, J. Sun, Z. Zhang, and H. Hua, "Vibration isolation characteristics of a nonlinear isolator using euler buckled beam as negative stiffness corrector: a theoretical and experimental study," *Journal of Sound and Vibration*, vol. 333, no. 4, pp. 1132–1148, 2014.

[4] F. Zhao, J. Ji, K. Ye, and Q. Luo, "An innovative quasi-zero stiffness isolator with three pairs of oblique springs," *International Journal of Mechanical Sciences*, vol. 192, p. 106093, 2021.

[5] L. Wu, Y. Wang, Z. Zhai, Y. Yang, D. Krishnaraju, J. Lu, F. Wu, Q. Wang, and H. Jiang, "Mechanical metamaterials for full-band mechanical wave shielding," *Applied Materials Today*, vol. 20, p. 100671, 2020.

[6] H. Fan, L. Yang, Y. Tian, and Z. Wang, "Design of metastructures with quasi-zero dynamic stiffness for vibration isolation," *Composite Structures*, vol. 243, p. 112244, 2020.

[7] C. Cai, J. Zhou, L. Wu, K. Wang, D. Xu, and H. Ouyang, "Design and numerical validation of quasi-zero-stiffness metamaterials for very low-frequency band gaps," *Composite structures*, vol. 236, p. 111862, 2020.

[8] D. M. Correa, T. Klatt, S. Cortes, M. Haberman, D. Kovar, and C. Seepersad, "Negative stiffness honeycombs for recoverable shock isolation," *Rapid Prototyping Journal*, 2015.

[9] T. Zhu, B. Cazzolato, W. Robertson, and A. Zander, "The development of a 6 degree of freedom quasi-zero stiffness maglev vibration isolator with adaptive-passive

load support," in *15th International Conference on Mechatronics Technology. URL: http://hdl. handle. net/2440/72548*, 2011.

[10] S. A. J. Hol *et al.*, "Design and optimization of a magnetic gravity compensator," in *4th International Conference of the European Society for Precision Engineering and Nanotechnology*, 2004.

[11] J. Janssen, J. Paulides, E. Lomonova, B. Delinchant, and J.-P. Yonnet, "Design study on a magnetic gravity compensator with unequal magnet arrays," *Mechatronics*, vol. 23, no. 2, pp. 197–203, 2013.

[12] H. Zhang, B. Kou, Y. Zhou, Y. Liu, Q. Ge, and Y. Shao, "Modeling and analysis of a large-load magnetic levitation gravity compensator," in *2019 22nd International Conference on Electrical Machines and Systems (ICEMS)*, pp. 1–5, IEEE, 2019.

[13] H. Zhang, B. Kou, Y. Jin, and H. Zhang, "Modeling and analysis of a new cylindrical magnetic levitation gravity compensator with low stiffness for the 6-dof fine stage," *IEEE Transactions on Industrial Electronics*, vol. 62, no. 6, pp. 3629–3639, 2014.

[14] R. Berkhof, "Vertical vibration isolation using permanent magnets," 2015.

[15] S. M. Mofidian and H. Bardaweel, "Theoretical study and experimental identification of elastic-magnetic vibration isolation system," *Journal of Intelligent Material Systems and Structures*, vol. 29, no. 18, pp. 3550–3561, 2018.

[16] G. Dong, X. Zhang, S. Xie, B. Yan, and Y. Luo, "Simulated and experimental studies on a high-static-low-dynamic stiffness isolator using magnetic negative stiffness spring," *Mechanical Systems and Signal Processing*, vol. 86, pp. 188–203, 2017.

[17] H. Zhang, B. Kou, Y. Jin, H. Zhang, and L. Zhang, "Research on a low stiffness passive magnetic levitation gravity compensation system with opposite stiffness cancellation," *IEEE Transactions on Magnetics*, vol. 50, no. 11, pp. 1–4, 2014.

[18] H. Zhang, B. Kou, and Y. Zhou, "Analysis and design of a novel magnetic levitation gravity compensator with low passive force variation in a large vertical displacement," *IEEE Transactions on Industrial Electronics*, vol. 67, no. 6, pp. 4797–4805, 2019.

[19] R. Argiro, "The design and experimental validation of a permanent magnet long-stroke gravity compensator," 2021.

[20] J. Janssen, "Extended analytical charge modeling for permanent-magnet based devices/practical application to the interactions in a vibration isolation system," 2011.